Cell Reports
Methods

Article

Dense optical flow software to quantify cellular contractility

Graphical abstract

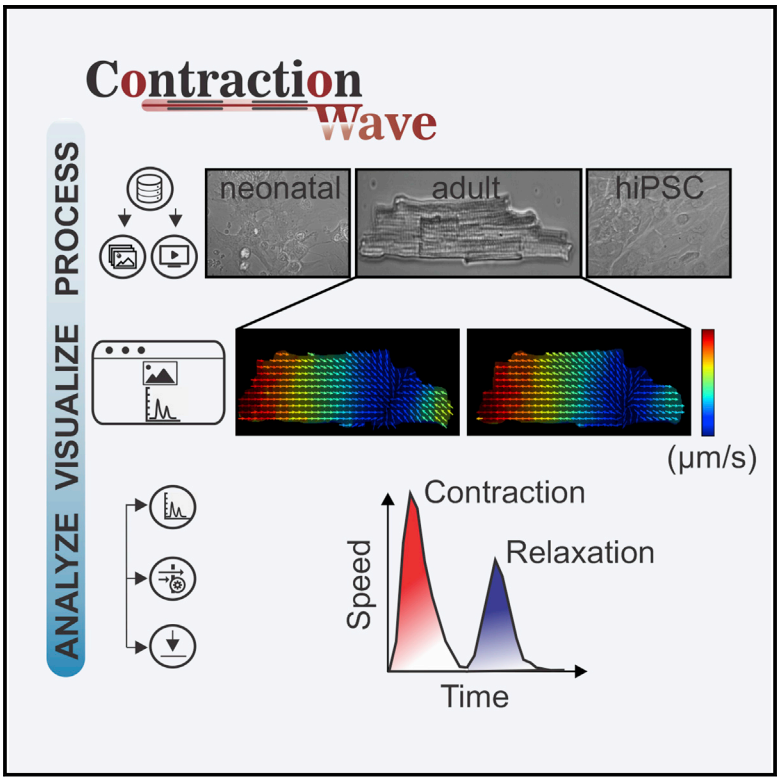

Authors

Sérgio Scalzo, Marcelo Q.L. Afonso, Néli J. da Fonseca, Jr., ..., Maria José Campagnole-Santos, Ubirajara Agero, Silvia Guatimosim

Correspondence

bira@fisica.ufmg.br (U.A.), guatimosim@icb.ufmg.br (S.G.)

In brief

Quantification of contractility is an important step in understanding cardiac disease. To meet this demand, Scalzo et al. develop CONTRACTIONWAVE, open-source software for large-scale analysis of cardiomyocyte contraction. Combining speed and flexibility, the pipeline provides a solution for laboratories and companies involved in drug screening and cardiac disease modeling.

Highlights

- Open-source Python software for large-scale analysis of cardiomyocyte contractility
- CW uses the dense optical flow algorithm to quantify contractility parameters
- CW provides a user-friendly interface designed for the non-specialist
- CW displays cellular images correlated to motion vectors and their graphical results

Scalzo et al., 2021, Cell Reports Methods *1*, 100044
August 23, 2021
https://doi.org/10.1016/j.crmeth.2021.100044

CellPress

Cell Reports Methods

CellPress
OPEN ACCESS

Article

Dense optical flow software to quantify cellular contractility

Sérgio Scalzo,[1,7] Marcelo Q.L. Afonso,[2,7] Néli J. da Fonseca, Jr.,[2,6] Itamar C.G. Jesus,[1] Ana Paula Alves,[3] Carolina A.T. F. Mendonça,[1] Vanessa P. Teixeira,[1] Diogo Biagi,[4] Estela Cruvinel,[4] Anderson K. Santos,[1] Kiany Miranda,[1] Flavio A.M. Marques,[5] Oscar N. Mesquita,[3] Christopher Kushmerick,[1] Maria José Campagnole-Santos,[1] Ubirajara Agero,[3,*] and Silvia Guatimosim[1,8,*]

[1]Departamento de Fisiologia e Biofísica, Instituto de Ciências Biológicas, Universidade Federal de Minas Gerais, Belo Horizonte, MG 31270-901, Brazil

[2]Departamento de Bioquímica e Imunologia, Instituto de Ciências Biológicas, Universidade Federal de Minas Gerais, Belo Horizonte, MG 31270-901, Brazil

[3]Departamento de Física, Instituto de Ciências Exatas, Universidade Federal de Minas Gerais, Belo Horizonte, 31270-901, Brazil

[4]PluriCell Biotech, São Paulo, SP 05508-000, Brazil

[5]Departamento de Física, Instituto de Ciências Naturais, Universidade Federal de Lavras, Lavras, MG 37200-900, Brazil

[6]Cellular Structure and 3D Bioimaging, European Molecular Biology Laboratory, European Bioinformatics Institute, Wellcome Genome Campus, CB10 1SA Hinxton, UK

[7]These authors contributed equally

[8]Lead contact

*Correspondence: bira@fisica.ufmg.br (U.A.), guatimosim@icb.ufmg.br (S.G.)

https://doi.org/10.1016/j.crmeth.2021.100044

MOTIVATION Quantification of cardiomyocyte contractility is an important step in understanding the cellular mechanisms involved in the pathogenesis of cardiac disease. However, accurate and reproducible measurements are hampered by several factors inherent to the software options currently available. These include limited ability to process large datasets, the inability to provide calibrated measurements of contractility speed, the absence of a unified and accessible computational package, the high cost of some programs, and often the need for advanced programming skills. Aiming to overcome these limitations, we developed CONTRACTIONWAVE, open-source Python software that provides high-performance algorithms for large-scale analysis of cardiac contraction.

SUMMARY

Cell membrane deformation is an important feature that occurs during many physiological processes, and its study has been put to good use to investigate cardiomyocyte function. Several methods have been developed to extract information on cardiomyocyte contractility. However, no existing computational framework has provided, in a single platform, a straightforward approach to acquire, process, and quantify this type of cellular dynamics. For this reason, we develop CONTRACTIONWAVE, high-performance software written in Python programming language that allows the user to process large data image files and obtain contractility parameters by analyzing optical flow from images obtained with videomicroscopy. The software was validated by using neonatal, adult-, and human-induced pluripotent stem-cell-derived cardiomyocytes, treated or not with drugs known to affect contractility. Results presented indicate that CONTRACTIONWAVE is an excellent tool for examining changes to cardiac cellular contractility in animal models of disease and for pharmacological and toxicology screening during drug discovery.

INTRODUCTION

According to the World Health Organization, cardiovascular diseases represent a significant cause of death worldwide (Mozaffarian et al., 2016). In order to develop new therapeutic strategies, many studies employ the isolated cardiomyocyte (CM) either as a platform for drug discovery (Lieben Louis et al., 2019; Nguyen et al., 2017) or as an *in vitro* model to investigate the underlying mechanisms of cardiac disease (Chen et al., 2018; Kodo et al., 2016; Schick et al., 2018). Isolated cardiac myocytes have also been widely used to answer basic questions about cardiac cellular physiology and to characterize changes

in the excitation-contraction coupling that occurs during disease development (Chen-Izu et al., 2007; Goméz, 1997; Song et al., 2005).

An important parameter for the analysis of the isolated CM is contractility, which provides information that reflects its cellular function. Measurements of contractility have been widely used for research on both adult and neonatal myocytes (Belostotskaya and Golovanova, 2014; Berger et al., 1994; Boudreau-Béland et al., 2015; Harary and Farley, 1960; Haworth et al., 1987; Hissa et al., 2017; Jesus et al., 2020; Penitente et al., 2014; Ramadan et al., 2018). More recently, human induced pluripotent stem cell-derived CMs (hiPSC-CMs) have been employed as a model for human cardiac disease and drug screening (Ballan et al., 2020; Birket et al., 2015; Gong and Sobie, 2018; Lahti et al., 2012; Lan et al., 2013; Ribeiro et al., 2015; Wang et al., 2014, 2019). The development of this new experimental model, although showing great promise, also brings some challenges to efficiently detect CM contraction dynamics. Measurements in adult myocytes are relatively simple due to their geometry and one-dimensional movement, whereas in neonatal CMs and hiPSC-CMs, the functional syncytium formed by the cells lacks well-defined borders and represents a challenge to acquire contractility parameters.

Evaluation of CM contractility can be achieved by using methods that capture cellular movements associated with cellular contraction and relaxation. These methods include well-established techniques, such as light diffraction (Leung, 1982), laser microscopy (Shevchuk et al., 2001), scanning ion conductance microscopy (Gorelik et al., 2006), and atomic force microscopy (Chang et al., 2013). However, these techniques usually require sophisticated instruments, a highly experienced analyst, high financial investments, and time-consuming experiments. In addition to these practical issues, these techniques also have the potential to cause cell damage. In the specific case of adult CMs, the most commonly used technique to study cellular contractility is the edge detection system that measures cell border movement (IonWizard Ionoptix, Steadman et al., 1988). Although widely used, this technique does not capture the movement of the whole cell area, but instead only analyzes a specific region of interest defined by the user, which can introduce bias to the results during acquisition and analysis processing (Delbridge and Roos, 1997).

The development of high-speed digital cameras and image-processing techniques allowed the emergence of new methodologies and significantly improved how data collection is performed for cellular contractility evaluation. Together with optical microscopes, these tools allow for a more accurate and non-invasive assessment of cellular contractility (Huebsch et al., 2015; Maddah et al., 2015), and have shown great promise for both basic and clinical research. Hayakawa et al. (2014) were the first to apply an optical flow methodology to access contraction cycles in CMs. By performing simultaneous measurements of cellular contractility and electrophysiological parameters, the authors demonstrated that the optical flow technique allows accurate quantification of CM contractility parameters that correlate well with the electrophysiology results. Subsequent image-based studies have characterized CM contractility parameters by using different algorithms based on optical flow (Czirok et al., 2017; Huebsch et al., 2015; Pointon et al., 2017). In addition, the authors assessed the effects of several drugs that modulate cellular contraction to reinforce the sensitivity and efficiency of this type of analysis. Recently, computational methods, available as ImageJ plugins (Schindelin et al., 2015), have been developed for quantitative assessment of CM contractile responses (Boudaoud et al., 2014; Grune et al., 2019; Pasqualin et al., 2016; Sala et al., 2018). Despite this progress, the field still lacks and would greatly benefit from a computational framework that can provide fast and accessible analysis of cellular contractility.

Here, we present CONTRACTIONWAVE, an open-source software written in the Python programming language (van Rossum, 1995; for more details see the User Manual provided as Methods S1) with a built-in user-friendly interface, which combines in a single platform a robust method to acquire, visualize, analyze, and quantify contractility parameters of cardiac cells at different developmental stages through image capture and optical flow. The high-performance algorithms can automatically process large data image files in a fast and accurate manner. In addition, CONTRACTIONWAVE presents an innovative way to simultaneously display cellular images obtained during a contraction-relaxation cycle correlated to motion vectors and their respective graph representation. Therefore, CONTRACTIONWAVE combines a high processing capability and flexibility with an interface designed for the non-specialist audience, providing a solution required by laboratories and biotech companies involved in drug screening and cardiac disease modeling.

RESULTS

CONTRACTIONWAVE measures contractility by time-lapse image analysis of individual CMs observed under bright-field microscopy. To acquire the cell movement, CONTRACTIONWAVE calculates contractility from generated images based on principles of optical flow, computing the dense optical flow as described by Farneback (2003).

Our implementation of the dense optical flow method has the advantage of reporting both the direction of movement in the form of oriented vectors and calibrated measurement of speed in μm/s. The method does not require a Gaussian filter to access cellular displacement, and the analysis is less sensitive to illumination conditions than the principle of pixel intensity (Hossain et al., 2010; Sala et al., 2018), which can influence contraction amplitude parameters.

CONTRACTIONWAVE workflow

Figure S1A provides an outline of the initial screen that allows the user to import and process large image datasets and analyze the results obtained. CONTRACTIONWAVE can process frames obtained from sequential images or video files (processing window, Figure 1). Most of the currently available software packages are only able to process image datasets one at a time. In contrast, CONTRACTIONWAVE is a multithreaded application, allowing the simultaneous processing of multiple, large datasets (processing window, Figure 1). Moreover, the progress of image processing can be followed in real time (Figure S1C) and data

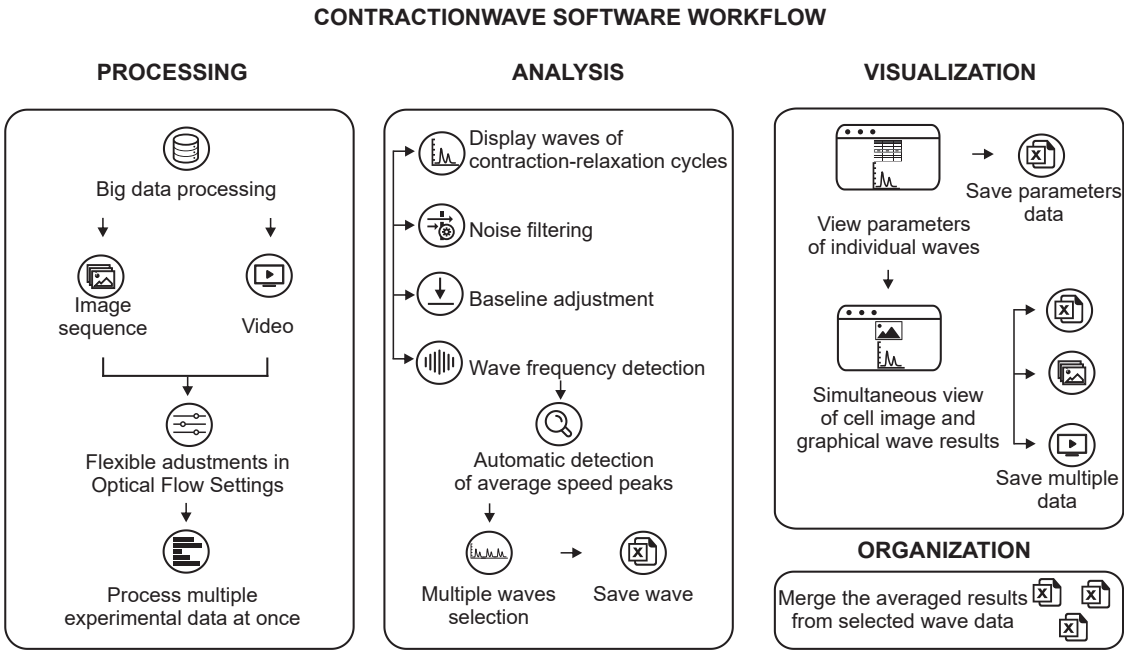

Figure 1. CONTRACTIONWAVE software workflow

CONTRACTIONWAVE comprises four steps to study cell contractility: data processing, data analysis, visualization, and results management. Processing: the program innovates with its capacity to process big amounts of data, from either images or videos, all at once. Analysis: the user can select the background noise and normalize the entire data to a new adjusted baseline. Then, the software algorithm is capable of automatically identifying the contraction-relaxation waves, also allowing fine adjustments. Subsequently, multiple waves can be selected to be further analyzed and the progress saved. Visualization: parameters of each wave can be visualized and selected. The cell and the graphical images can be simultaneously visualized and the final results saved. Organization: the averaged results from multiple waves can all be merged in a single table and saved.

analysis can be done concurrently with the processing of new datasets.

An interesting feature of our software is the flexibility to adjust the program settings. Although CONTRACTIONWAVE has an optical flow default setting that can be used for most cellular experiments, the program allows the user to adjust and choose the best experimental parameters (Figure S1B) depending on the image quality or cell type. To provide the measurements of cell movement in physical units (μm/s) the user needs to insert experimental settings, such as frames per second and pixel size (μm).

Once movement information is extracted from the video files, the user starts the contractility analysis by clicking on the menu "start analysis" (Figure S1A). The calculated speed versus time data are initially shown in a plot that corresponds to contraction-relaxation cycles (waves), which can be selected by clicking and dragging an interval to start the analysis (Figure S2A). The analysis workflow is divided to: (1) display waves of contraction-relaxation cycles; (2) noise filtering; (3) baseline adjustment; and (4) wave frequency detection (see analysis window, Figure 1). These parameters are found in the "wave detection window" (Figure 2A). A typical speed versus time profile corresponding to contraction-relaxation cycles, generated from the optical flow processed images, is presented in Figure 2A (top panel). For analysis purposes, CONTRACTIONWAVE gives the user the option to choose a single contractile cycle or the average of multiple cycles. In the wave detection window, once the selection is made (top panel, orange area, Figure 2A), a second plot showing a zoomed version of the selected interval is displayed (bottom panel, Figure 2A) to assist the user to choose the detected waves of interest to be analyzed.

In addition, CONTRACTIONWAVE provides the option to decrease the background noise by selecting the "decrease noise cutoff" box (top box, Figure 2A). The calculated noise value is then plotted as a blue line as shown in the graphical representation on the bottom panel of Figure 2A (see section 5.2.1 of the User Manual provided as Methods S1 for more details).

Despite all these detection steps, waves from datum groups with noisy oscillations that are close to the baseline signal values may still be difficult to assign from the speed data calculated by the optical flow algorithm. These particularly arise from multidirectional contraction-relaxation dynamics, such as those found in neonatal-CMs and hiPSC-CMs in culture. To minimize noisy waves, at the pre-analysis settings, the user can select smooth-denoise algorithms on Data Options > smooth-denoise (see Figure 34, Section 5.3, from User Manual provided as Methods S1).

Another important parameter that can be acquired is the cell wave frequency, which can be done by simply clicking on subplot-mode > fast Fourier transform. Once the data (top, Figure S2B) is analyzed, the corresponding cell frequency value will be represented by the highest amplitude density peak obtained, as shown by the purple circle (see black arrow) in the bottom panel of Figure S2B. In this example, the cell wave frequency is 0.9 Hz.

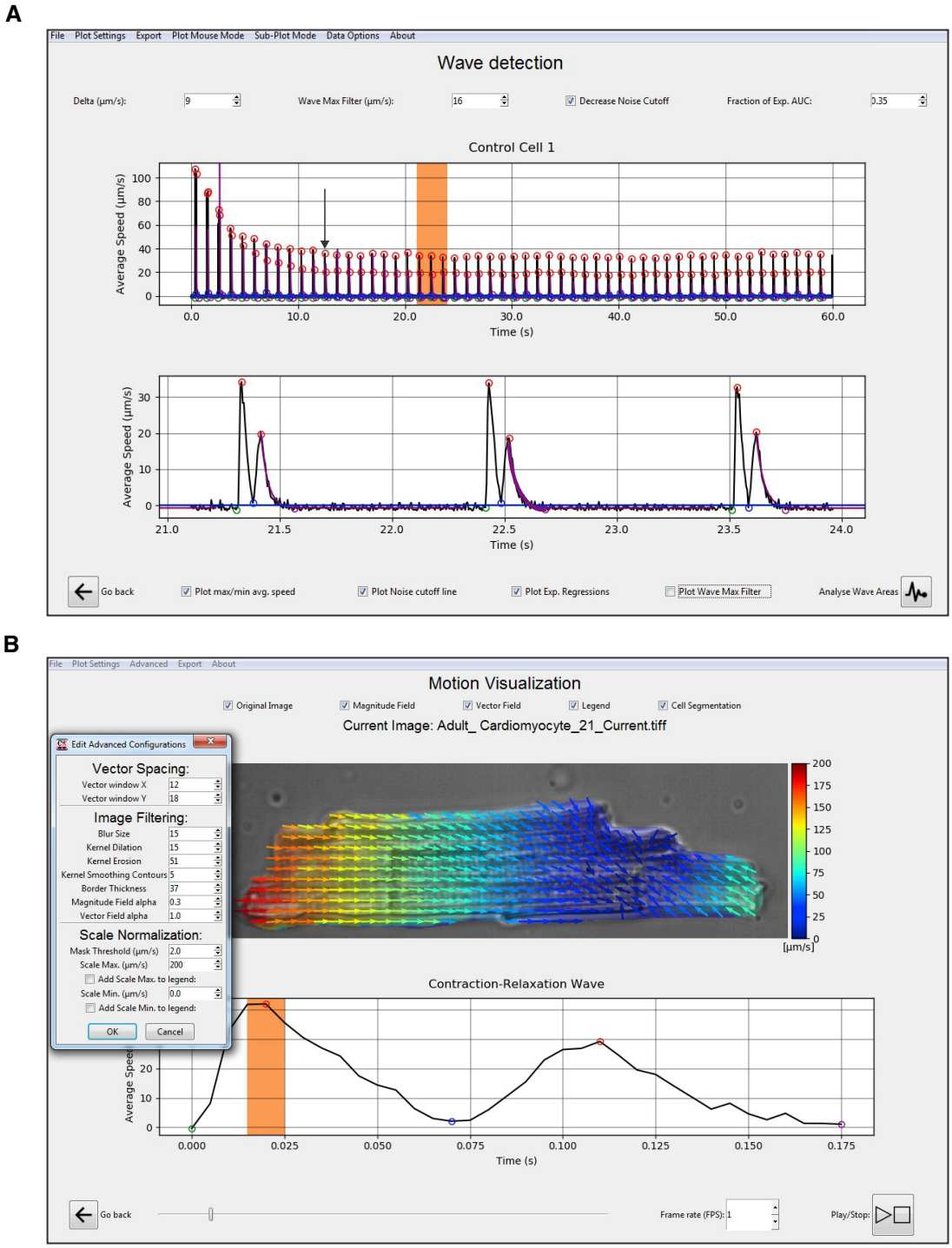

Figure 2. CONTRACTIONWAVE basic functions and applications

(A) CONTRACTIOWAVE has a robust analysis window that allows the user to select multiple datum intervals to extract the contractility parameters. The program can automatically detect the contraction-relaxation average speed waves, and also allows fine adjustments to find the correct wave peaks (top). The black arrow indicates the start of the steady state. To assist the selection of single or multiple peaks, a zoomed version of the plot is also displayed (bottom). The purple line shows the exponential regression fit of the relaxation speed decay phase.

(B) CONTRACTIONWAVE innovates on the way the cell is visualized, as both the cell image (top) and the contraction waves (bottom panel) are displayed simultaneously. Moreover, a dynamic analysis of the image sequence coordinated with the magnitude and motion vectors of the contractility movement is also available (the orange area on the bottom panel highlights the time in which the upper cell image was acquired). CONTRACTIONWAVE allows detection adjustments on the "advanced" options (box) and also filters the displayed magnitudes by a given speed threshold by using the "mask threshold" function.

Once the contractile cycles are selected (Figure 2A, orange box), the user can visualize in the following window (wave parameters, Figure S2C) each of the previously selected beats and calculate the average. As shown in Figure S2C (bottom), the average speed for a contraction-relaxation cycle provides two subsequent waves: a major wave that corresponds to contraction, and a minor one that reflects the relaxation dynamics. CONTRACTIONWAVE can automatically find the contraction-relaxation average speed peaks, and the acquired and parameterized data will contain five points: (1) contraction initiation; (2) maximum contraction speed (MCS); (3) minimum contraction speed; (4) maximum relaxation speed (MRS); (5) return to baseline. To detect all points, the Delta value (μm/s) should be set as half of the minimum difference between baseline points and the MRS point. The Delta value box can be found in the wave detection window (top left, Figure S2B).

Since cell relaxation ends with a slow decay that can be difficult to distinguish from background noise, detecting the endpoint of the contractility wave (fifth point in Figure S2C) is usually a challenge during the data analysis process. To appropriately detect the end of one contraction-relaxation cycle, CONTRACTIONWAVE fits an exponential function from peak relaxation down to baseline (see the purple line in Figure 2A). A customizable stopping criterion is then used for determining the end of a wave. For details regarding default recommended settings, see Figure 5 in section 3.3 from the Quickstart Guide or Figure 32 in section 5.2.3, both in the User Manual provided as Methods S1. Alternatively, the user can use one of several fixed decay time points (T10%, T20%, T30%, T40%, T50%, T60%, T70%, T80%, and T90%), which are exported together with the analyzed data. The points indicate the time at which the relaxation speed decayed to a certain percentage of its peak amplitude. Some decay times are represented in Figure 3B.

After the average speed peaks are properly assigned and selected, the time, speed, and area parameters for each detected wave can be then visualized and exported in the subsequent window by clicking the appropriate boxes on the top panel of Figure S2C. After selecting one wave, the user can click on "motion visualization" (bottom right box in Figure S2C) to visualize data (Figure 2B).

Another innovation introduced in CONTRACTIONWAVE is a visualization feature that allows simultaneous viewing of the cell image and the contraction waves (visualization window, Figures 1 and 2B). No other program allows for complete and integrated visualization of a cellular movement, a resource that CONTRACTIONWAVE achieves by drawing motion vectors, correlating the movement throughout the image to their respective wave points on the contraction-relaxation graph (Figure 2B). In Figure 2B (bottom) the orange box represents the respective wave point in which the image was acquired.

Visual and numerical detection of contraction

To validate the system, we investigated the contractility of three well-established cardiac cell type models: (1) acutely isolated adult mice or rat ventricular myocytes (adult-CMs); (2) cultured neonatal-CMs; and (3) hiPSC-CMs (see the STAR Methods for more details). Unlike other neonatal and hiPSC-CM systems that form a syncytium *in vitro*, the adult-CM is a much simpler subject composed of a single cell with robust contraction dynamics. Therefore, we first tested the CONTRACTIONWAVE functionality by using adult-CMs that were electrically stimulated to contract repeatedly at 1 Hz. A typical sequence of average speed waves obtained from an adult-CM is shown in Figure 2A. Typically, the maximum speed is greatest for the first contractions in the sequence and then gradually decays over time until it stabilizes at a steady-state speed value (see black arrow in Figure 2A). After reaching the steady state, we can analyze the contraction-relaxation dynamics. Representative images acquired during each phase of the speed wave are shown in Figure 3Ai–v.

Extraction of movement associated with cellular contractility occurs through analysis of sequential pairs of images that are processed with the dense optical flow algorithm by using all pixels in the image. This allows the program to identify pixel displacement and calculate its magnitude and direction. The final motion magnitude is obtained from the pixel displacement magnitude mean for each image, converted to the real speed, by using the multiplication of the frame rate and the pixel resolution (set by the user), then plotted on a time function graph (see the STAR Methods for more details). This process allows the detection and generation of the total magnitude displacement (Figure 3A, magnitude field) and motion vectors (Figure 3A, vector field). In Figure 3A, membrane displacement speed is represented on a visual and numerical intensity scale. Under resting conditions, before electrical stimulation, motion vector intensity is low, with an average speed close to zero (Figure 3Ai). After the electrical stimulus, the cellular contraction starts and can be visualized by the increase in motion vector intensity. The cell then reaches its MCS (Figure 3Aii). After MCS, vector intensity decreases, approaching the zero speed, representing the point of maximum cell shortening (Figure 3Aiii). When relaxation starts, the vector motion direction changes, and the average vector motion speed increases until it reaches the MRS (Figure 3Aiv). After the end of a relaxation cycle, the vector intensity and average speed return to the basal level (Figure 3Av).

As shown in the merged panel (transmitted light image, magnitude field, and vector field) illustrated in Figure 3A, CONTRACTIONWAVE can detect membrane displacement throughout the whole cellular area, and spatial resolution was limited only to the microscope and camera used. From the generated data, the mean magnitude speed can be plotted for each frame as a function of time (Figure 3B). This allows the quantitative analyses of parameters that reflect the dynamics of the entire CM contraction-relaxation cycle. All points identified with roman numerals in Figure 3B correspond to the phases of the contraction cycle defined in Figure 3A. A summary of all contraction/relaxation parameters obtained by CONTRACTIONWAVE is presented in Figure 3B and can be divided into three categories: speed, time, and area.

Sometimes the correct identification of the wave is difficult. This normally occurs with immature cells and can be caused by noise or even by the fact that there are cells for which the MRS is greater than the MCS. To circumvent this problem, CONTRACTIONWAVE has a pipeline in the wave detection window (data options > contraction amplitude) (Methods S1: User Manual, section 5.8, Contraction amplitude) that allows the user to visualize the entire contraction-relaxation cycle along with a corresponding single peak that represents the amplitude contraction.

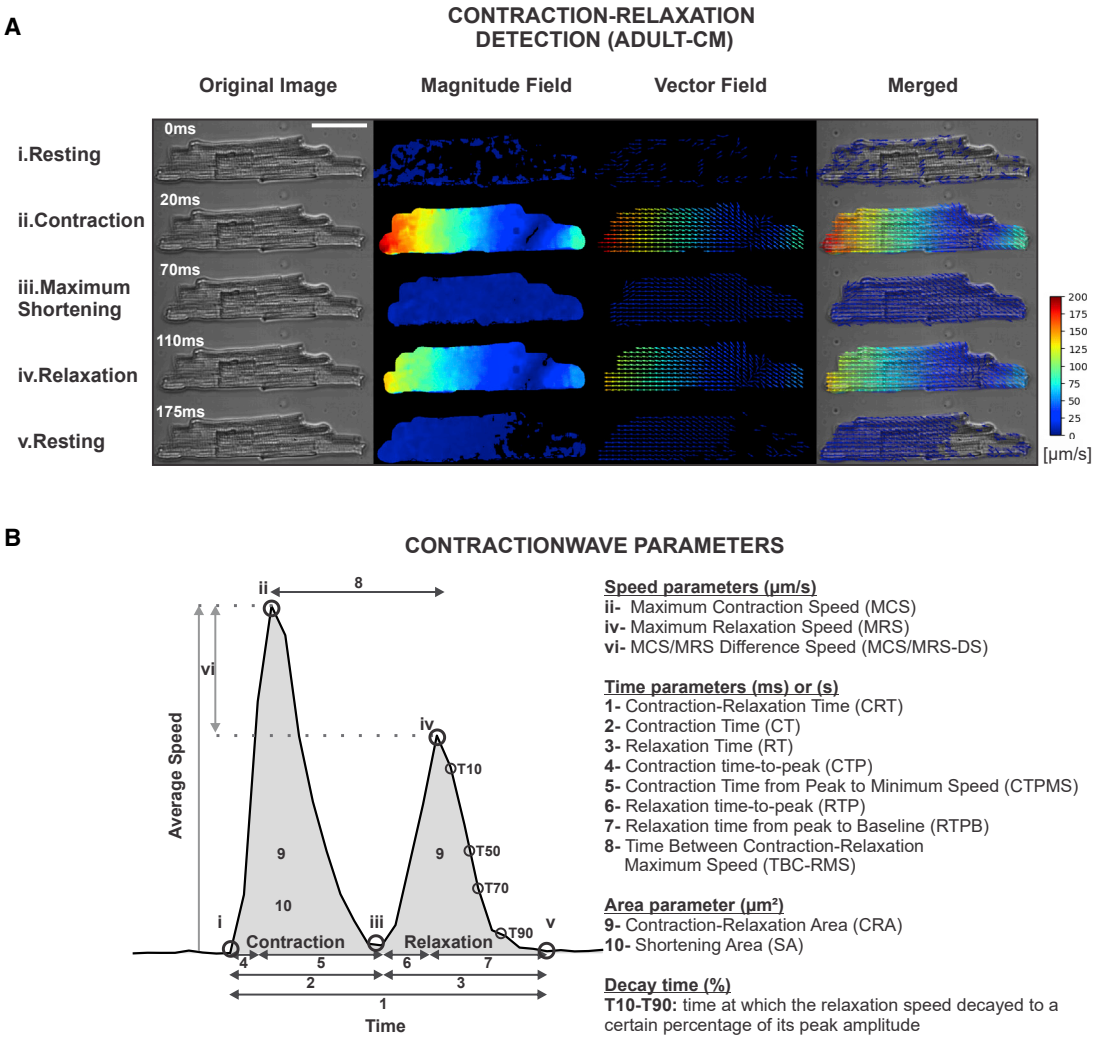

Figure 3. CONTRACTIONWAVE enables the user to acquire data regarding membrane kinetics of CMs during contraction-relaxation cycles through image capture

(A) Sample images show the membrane movement detection by the magnitude and vector fields with visual and numerical intensity scale detection during a contraction-relaxation cycle in adult-CMs. Scale bar, 40 µm.

(B) Left, sample average speed wave acquired from one contraction-relaxation cycle in an electrically stimulated CM. All points identified with roman numerals in (B) correspond to the phases of the contraction cycle defined in (A). Right, a summary of CONTRACTIONWAVE parameters obtained during a contraction-relaxation cycle.

Application of CONTRACTIONWAVE in adult myocyte contractility

CONTRACTIONWAVE was idealized and developed to eliminate the limitations that optical edge detection and segmentation methods have, such as the requirement for proper cell alignment and cell rotation during the acquisition process for adult-CMs (Delbridge and Roos, 1997; Ren and Wold, 2001). To test the effectiveness and sensitivity of our method we exposed the cells to drugs that have well-defined effects on contractility parameters. Adult-CMs were subjected to treatment with either isoproterenol (ISO) (100 nmol L^{-1}) or verapamil (VERA) (100 nmol L^{-1}). Isoproterenol is a β-adrenergic agonist that significantly enhances CM contractility by increasing the average speed, and the extent of shortening length, thus decreasing the time required for contraction and relaxation (Butler et al., 2015; Harmer et al., 2012). Verapamil is a calcium channel blocker, widely used for the treatment of cardiac arrhythmias (Bourgonje et al., 2013), as well as an antihypertensive, because of its negative inotropic and chronotropic effect in the cardiac system (Harmer et al., 2012; Stern et al., 1986). Figure 4Ai–ii shows the sample spatial images and the average speed traces, respectively, recorded from cells stimulated at 1 Hz and treated with isoproterenol or verapamil for 60 s. Figure 4Aiii shows a zoomed view of one average speed trace acquired from one cycle of contraction-relaxation. Figures 4B–4D displays concentration-response analysis for the effects of isoproterenol and verapamil on contractility parameters of adult-CMs, from three independent experiments. As shown in Figure 4B, both ISO and VERA reduced contraction and relaxation times, with more

CellPress
OPEN ACCESS

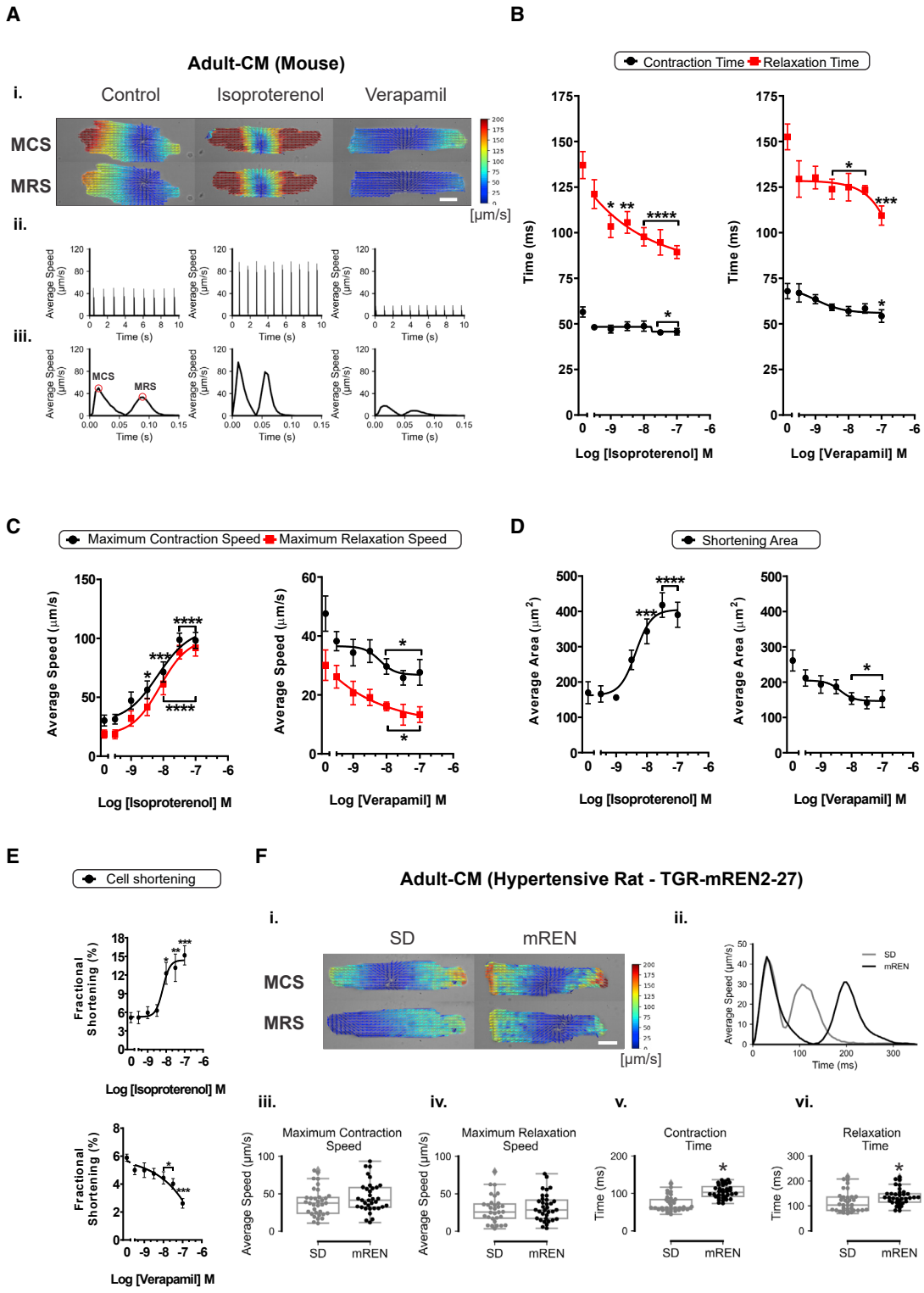

Figure 4. CONTRACTIONWAVE motion and graphical detection of contractility effects in adult-CMs from mice and TGR-mREN2-27 rats

(A) (i) Adult mouse CM cell displacement speed displayed in magnitude and vector fields with visual and numerical intensity scale detection during maximum contraction speed (MCS) and maximum relaxation speed (MRS) in response to isoproterenol (100 nmol L^{-1}) or verapamil (100 nmol L^{-1}) treatment. Scale bar, 20 μm. (ii) Average speed graph recorded from CMs stimulated to contract at 1 Hz. (iii) A single contraction-relaxation cycle was obtained under the effects of isoproterenol or verapamil treatments on CMs.

(legend continued on next page)

pronounced effects on relaxation time. Moreover, ISO increased maximum contraction and relaxation speed (Figure 4C) and shortened the area (Figure 4D) of adult-CMs in a concentration-dependent fashion. Opposite effects were observed when the cells were treated with VERA (Figures 4C and 4D). All contraction parameters acquired for adult-CMs treated with different concentrations of ISO and VERA are presented in Table S1. Of note, the data analysis does not require the user to manipulate the image as the software can process the entire image as it is generated by the experiment.

Another feature of CONTRACTIONWAVE is the possibility to acquire the shortening percentage of cell length for adult-CMs. In the advanced window of the Motion Visualization (Advanced > Export cell length data—Methods S1: User Manual—section 7.4 Figure 70), the user can open a new window to measure the shortening percentage of cell length (Figure S3). The window shows the wave selection box with the previously selected contraction-relaxation wave (blue bar on Figure S3A, left side) and its respective graph (Figure S3A, right side). CONTRACTIONWAVE uses the cell segmentation process to obtain the cell border length and apply the filters to find the best segmentation for the cell (Figure S3B). The data can be visualized and the graph plotted in real time (Figure S3C). Then, the analyzed wave data can be exported. To validate our segmentation method, we have performed shortening percentage of cell length analysis by using adult-CMs treated or not with isoproterenol and verapamil. As shown in Figure 4E, ISO increased the shortening percentage of cell length of adult-CMs, whereas VERA reduced it. Taken together, our data show that CONTRACTIONWAVE can reliably and efficiently process and analyze data from adult-CMs, detecting differences in contractility parameters under drug effects. This sensitivity, for instance, allows the investigation of drugs that can be cardioprotective, as well as the variation that occurs in relation to existing cardiac pathologies.

CONTRACTIONWAVE applicability in a rat model of hypertension

Contractility defects are a common feature in animal models of hypertension (Jesus et al., 2020; Kovács et al., 2016). Here, we used a well-characterized rat model of hypertension caused by genetic overexpression of renin in extrarenal tissues, the TGR (mREN2)27 rat (Langheinrich, 1996; Mullins et al., 1990). An important feature of mREN CMs is the increase in cellular area characteristic of cardiac hypertrophy (Jesus et al., 2020). Given that CONTRACTIONWAVE acquires the mean of the magnitude speed, the greater the size difference between the compared cells, the lower the sensitivity will be to acquire a difference that might exist. Thus, this can be a problem when measuring data from hypertrophic mREN myocytes when compared with Sprague-Dawley (SD) rat myocytes. To circumvent this problem, we implemented a pipeline by using a new filter (magnitude thresholding) (for details, see Methods S1: User Manual—section 7.3, Magnitude thresholding filter).

Figure 4Fi–ii shows CM images with motion vectors and the comparison of the average speed trace of SD and mREN myocytes. As shown in Figure 4Fiii–iv, there is no difference in maximum speed contraction or relaxation between SD and mREN myocytes. On the other hand, CONTRACTIONWAVE detected a significant increase in contraction and relaxation times in mREN myocytes when compared with SD cells (Figure 4Fv–vi). The contraction parameters are detailed in Table S2. These results extend previous findings (Jesus et al., 2020) by showing in more detail the cellular movement through vector fields along with the whole cell.

CONTRACTIONWAVE validation in neonatal-CM culture and hiPSC-CMs

Cardiomyocytes derived from different developmental stages show functional and structural differences. CONTRACTIONWAVE was designed to acquire contractility parameters in CMs under several experimental conditions during different maturation and cellular developmental stages. hiPSC-CMs and neonatal-CMs are immature cells that show distinct morphological and structural organization features compared with adult ventricular myocytes (Bedada et al., 2016; Khan et al., 2015; Li et al., 2017; Rohr et al., 1991). This structural lack of maturity affects CM contractility, which is considerably less robust than in adult CMs and poses a challenge for its acquisition and analyses. Moreover, hiPSC-CMs and neonatal-CMs are self-organized into a syncytium and exhibit spontaneous contraction (Bedada et al., 2016; Li et al., 2017).

HiPSC-CMs have been explored by different techniques to obtain cellular dynamics of contraction and relaxation (Czirok et al., 2017; Huebsch et al., 2015; Maddah et al., 2015; Pointon et al., 2017). However, their application as a routine in research and clinical centers remains a challenge, either due to implementation difficulties or because there is still a missing tool with a large processing capability combined with an interface designed for a non-specialist audience. CONTRACTIONWAVE provides a reliable, fast, and accessible approach for processing and analyzing contractility dynamics in these cellular types, from the image to the final results set.

Using CONTRACTIONWAVE, we determined the average speed of contraction and relaxation cycles in hiPSC-CMs (Figures 5 and S4) and neonatal-CMs (Figure 6) under basal control conditions and after incubation with ISO and VERA. Figure 5A shows sample spatial images that detect all hiPSC-CMs syncytial movement, which allows the user to extract the average speed traces from multiple contraction-relaxation cycles (Figure 5B). To have a better view, at a single-wave level, on

(B) Acute treatment with ISO and VERA induced a significant decrease in all-time parameters in CMs.
(C–E) (C) The cells treated with VERA presented a decrease of MCS and MRS, whereas ISO induced a significant increase in these parameters. ISO and VERA induced opposite effects on the shortening area (D) and fractional shortening (E).
(F) (i) SD and mREN cell displacement speed displayed in magnitude and vector fields with visual and numerical intensity scale detection during MCS and MRS. Scale bar, 20 μm. (ii) Graphical comparison of SD and mREN cells during one contraction-relaxation cycle. (iii)–(iv) SD and mREN CMs show similar MCS and MRS. (v)–(vi) mREN cells show an increase in contraction and relaxation time when compared with SD. For each cell, we analyzed a minimum of 10 events (each event corresponds to one contraction-relaxation cycle) and the results represent the average of these events. The results are expressed as means ± SE from an average of 30 cells from each experimental group. *$p < 0.05$, **$p < 0.01$, ***$p < 0.001$, ****$p < 0.0001$ compared with the control.

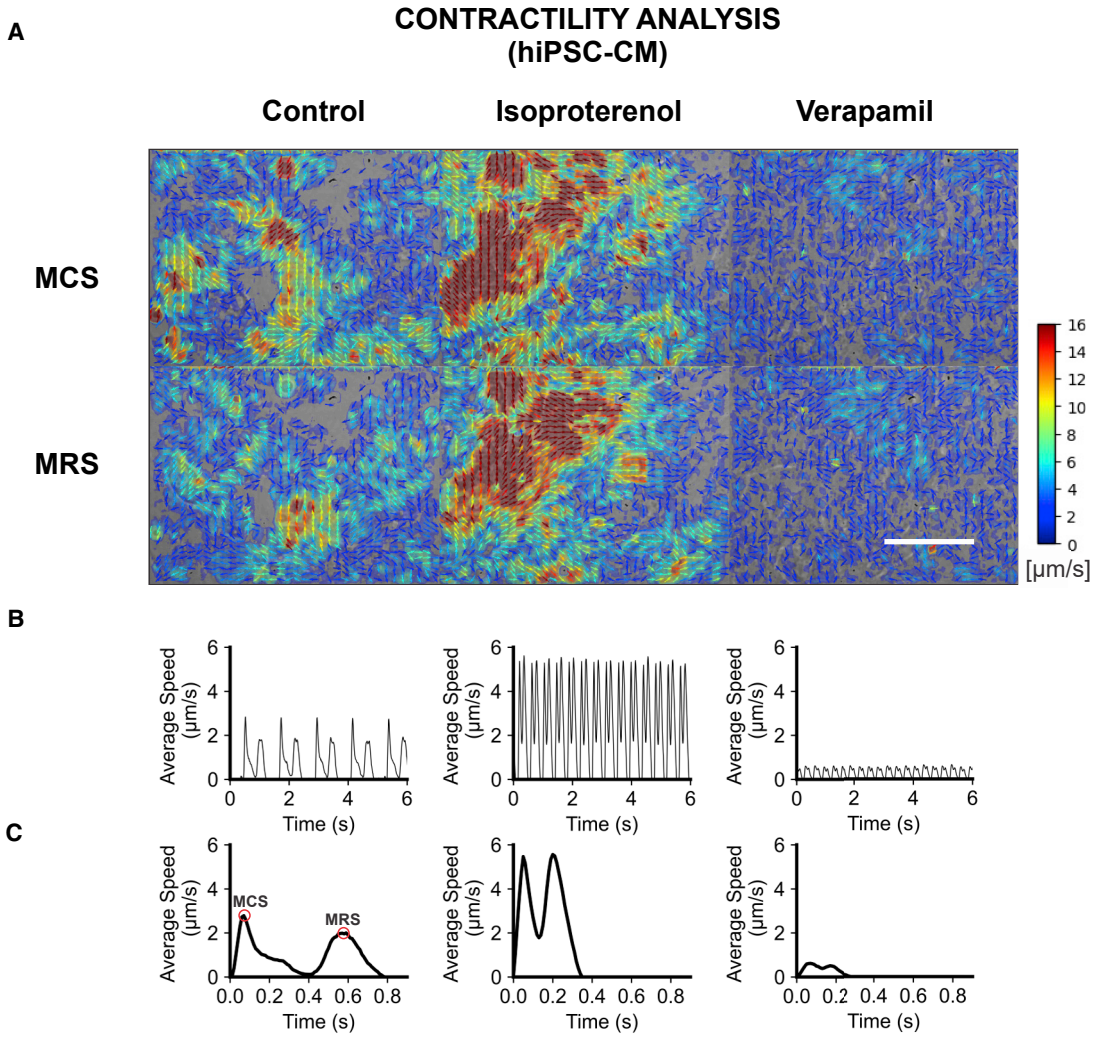

Figure 5. CONTRACTIONWAVE motion and graphical detection of isoproterenol and verapamil effects in hiPSC-CM contractility

(A) hiPSC-CM maximum displacement speed in visual and numerical intensity scale detection obtained from cells treated with isoproterenol (100 nmol L^{-1}) or verapamil (100 nmol L^{-1}). Scale bar, 50 μm.

(B) Graphical detection of average speed with treatments of isoproterenol or verapamil.

(C) Comparison of drug-induced changes during one contraction-relaxation cycle. MCS, maximum contraction speed; MRS, maximum relaxation speed. See also Figure S4.

treatment with ISO and VERA, the graph of each specific wave was plotted in Figure 5C. ISO and VERA effects on hiPSC-CMs also occurred in a concentration-dependent fashion and showed opposite results for both speed-dependent parameters (Figure S4A) and average shortening area (Figure S4B), as we would expect for these drugs. As previously reported in the literature (Hayakawa et al., 2014), a comparable decrease in contraction and relaxation times was observed upon treatment with ISO and VERA (Figure S4C). Moreover, ISO and VERA increased the beating frequency of hiPSC-CMs (Figure S4D). Taken together, these results confirm the versatility of our system, providing the user the possibility to obtain a visual and quantitative assessment of different contractile cell types by subtle modifications.

Likewise, Figure 6A shows that CONTRACTIONWAVE efficiently detects the difference of cellular contractility from ISO and VERA neonatal-CM-treated groups, through membrane displacement and generation of motion vectors (Figure 6Ai—iii). Moreover, the analysis shows that both ISO and VERA significantly decrease contraction and relaxation times, respectively, of neonatal-CMs in a concentration-dependent manner (Figure 6B). As expected for these drugs, treatment with ISO induced an increase in speed-dependent parameters (Figure 6C) and CM shortening area (Figure 6D), whereas a decrease was observed for VERA-treated cells. In addition, CONTRACTIONWAVE detected the self-rhythm of neonatal-CMs treated or not with the drugs. Opposing results of ISO and VERA were also observed when the beating frequency of neonatal-CMs was analyzed (Figure 6E).

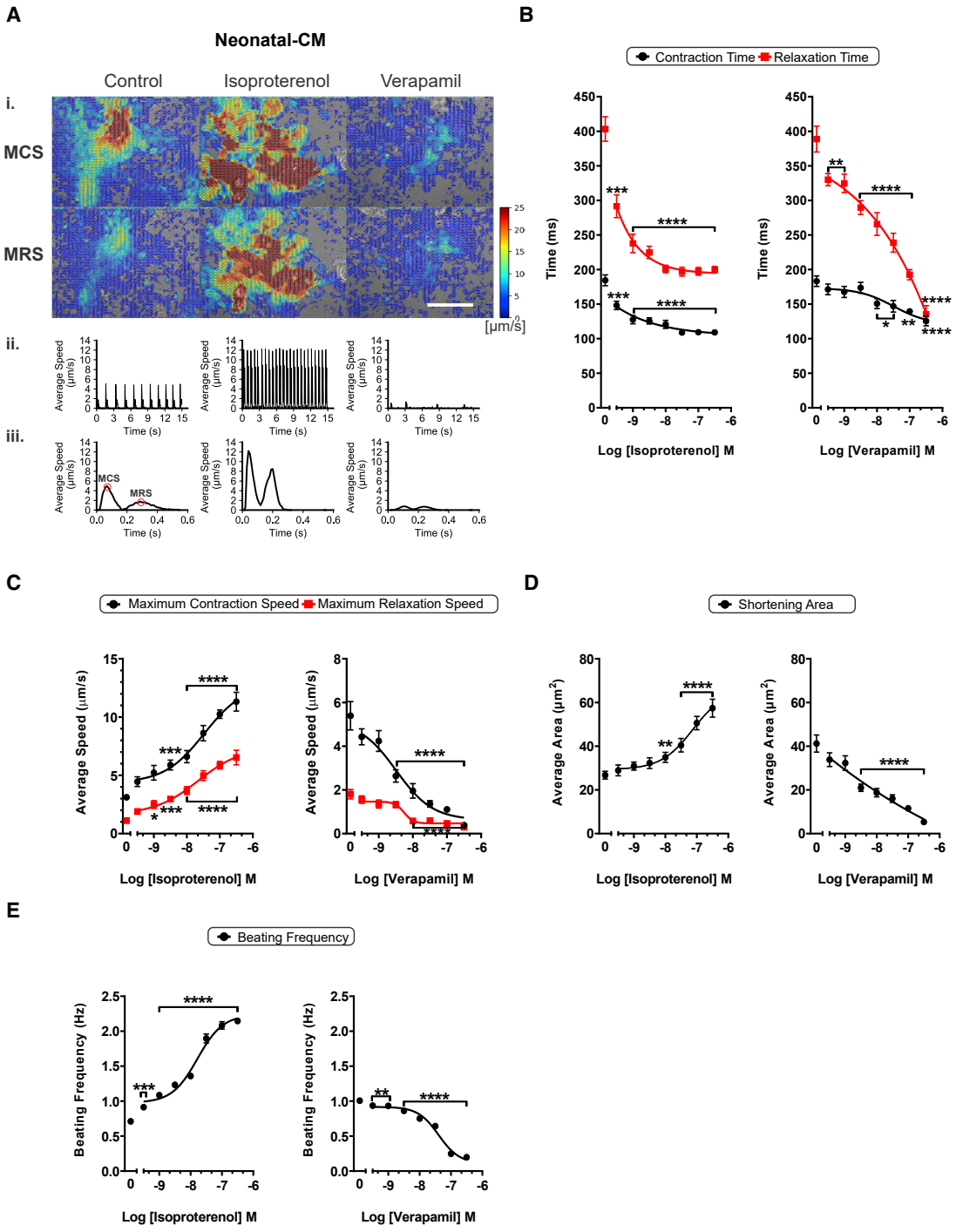

Figure 6. CONTRACTIONWAVE motion and graphical detection of isoproterenol and verapamil effects in neonatal-CM contractility

(A) (i) Neonatal-CM cell displacement speed in visual and numerical intensity scale detection during contraction-relaxation cycles obtained from effects of isoproterenol (100 nmol L^{-1}) or verapamil (100 nmol/L^{-1}) treatments. Scale bar, 50 μm. (ii) Graphical detection of average speed modifications recorded from isoproterenol or verapamil-treated neonatal-CMs. (iii) Comparison of drug-induced changes during one contraction-relaxation cycle.

(B) Acute treatment with ISO and VERA induced a significant decrease of contraction and relaxation time parameters in neonatal-CMs.

(C) The cells treated with VERA presented a decrease of MCS and MRS, whereas ISO induced a significant increase in these parameters.

(D) Similarly, ISO and VERA induced opposite effects on the shortening area.

(legend continued on next page)

The contraction parameters for both hiPSC-CMs and neonatal-CMs upon treatment with different concentrations of the drugs are presented in Tables S3 and S4, respectively.

To summarize our findings, Table S5 provides a comparison of maximum fold change in the contraction and relaxation speeds, and in the shortening area parameters between adult-CMs, neonatal-CMs, and hiPSC-CMs treated with ISO or VERA. As shown in Table S5, hiPSC-CMs show a weaker response to ISO in terms of contraction and relaxation speed maximum fold changes when compared with adult-CMs and neonatal-CMs. This finding shows an improved β-adrenergic response in neonatal cells when compared with hiPSC-CMs and indicates a difference in maturity between these two cell types. Despite the similar maximum fold change values shared by adult-CMs and neonatal-CMs, the former exhibited a lower half-maximal effective concentration confirming the stronger response of these cells to ISO. This is consistent with the fact that hiPSC-CMs and neonatal-CMs present immature β-adrenergic receptor signaling compared with adult-CMs (Jung et al., 2016; Slotkin et al., 1995). Yet, both neonatal-CMs and hiPSC-CMs showed a much stronger response to VERA compared with adult-CMs, with more pronounced inhibitory contraction effects observed in neonatal cells. Likewise, neonatal-CMs and hiPSC-CMs showed a reduced half-maximal inhibitory concentration to VERA for the MCS compared with adult-CMs. These differences reflect, at least in part, the high dependency of immature cells to the sarcolemmal Ca^{2+} cycling and the presence of immature Ca^{2+} release units (Korhonen et al., 2009; Louch et al., 2015). Overall, these data reinforce the sensitivity of our software to detect cellular differences in contractile responses to distinct drugs.

CONTRACTIONWAVE: A summary of its innovations and applications

We are aware of six other software programs available to analyze CM contractility (IonWizard Ionoptix; Boudaoud et al., 2014; Grune et al., 2019; Maddah et al., 2015; Pasqualin et al., 2016; Sala et al., 2018). Although these programs have enjoyed some success, none of them has engaged the large cardiac community. Several factors might explain this lack of engagement. For example, most work as ImageJ plugins, which might inhibit users looking for a turn-key solution. In addition, the two that have their user interface require payment, allowing only limited free use for testing. Furthermore, some have not demonstrated the ability to acquire contractions from hiPSC-CMs, thus limiting an important segment of the potential user community. Finally, these other programs do not have the multiprocessing window to analyze large amounts of data in parallel, as required for drug screening tests. In contrast, all these features are combined in CONTRACTIONWAVE. An extended summary of CONTRACTIONWAVE features is presented in Table S6.

CONTRACTIONWAVE provides an innovative solution for the high processing capability and flexibility required to quantify cardiac cell biomechanics and motility kinetics during the contraction-relaxation cycle. CONTRACTIONWAVE uses the dense optical flow algorithm which is less sensitive to the selection of "window size" when compared with older optical flow methods. This implies that significant changes in the optical flow parameters are not required to be optimized for each similar application. In addition, the second advantage of this algorithm is that it computes the displacement for all the pixels in the image, increasing sensitivity. One differential of CONTRACTIONWAVE compared with other available programs starts from how the data can be obtained, as the program allows a large amount of data to be processed at once through the multiprocessing window. This feature allows the user to process videos simultaneously, allocating the processes in different threads that are executed in parallel, improving performance when analyzing multiple datasets by factor N–1, where N is the number of CPU cores available. Moreover, high-performance algorithms were created to access the contractility graph, allowing the user to process automatically as well as to make fine and important adjustments that provide greater confidence in the acquisition of contractility parameters. Furthermore, the whole program was designed in a user-friendly interface that opens a wide and flexible manner for the graphical and image data to be analyzed. The noteworthy applicability of CONTRACTIONWAVE is the potential to be used for a better characterization of any contractile cell, by simply changing the optical flow parameters. In addition, the visualization of the processed results is displayed in an innovative way, as the program shows the correlated motion vectors and their respective graphs. Finally, CONTRACTIONWAVE was built in the Python programming language, which is one of the largest programming collaborative communities, facilitating improvements and increments to the program over time. In conclusion, CONTRACTIONWAVE is a versatile and robust platform, with unique abilities that set it apart from currently available software.

Limitations of study

CONTRACTIONWAVE uses the optical flow method that has arbitrary binning factors or thresholds, which can impose some limitations to data analysis. To bypass this potential issue, we provide default and flexible adjustments of these settings allowing calibrated measurements of contractility velocity (μm/s) that can be used on the majority of cellular experiments. An inherent limitation to all optical flow methods is that it captures the root-mean-square contraction velocity. These values reflect both random movements, corresponding to the baseline noise in our measurements, and additional movement associated with contraction and relaxation. Although this average does not directly reflect heart muscle contraction, it represents all cell displacements associated with contraction and relaxation and correlates with shortening speed at different cell stages and under different experimental conditions.

CONTRACTIONWAVE is a versatile, high-performance software capable of analyzing CM culture from basic research, such as neonatal-CMs and adult-CMs from various animal

(E) Both treatments show opposite effects on the cellular beating concentration-response curves. From each cell region, we analyzed a minimum of 10 events (each event corresponds to the contraction-relaxation cycle) and the results represent the average of these events in the presence or not of ISO and VERA. The results are expressed as means ± SE from an average of 20 cell regions from each experimental group. *$p < 0.05$, **$p < 0.01$, ***$p < 0.001$, ****$p < 0.0001$ compared with the control.

models to clinical research, as in the use of hiPSC-CMs. Its ability to acquire contractility data from hiPSC-CMs is crucial to obtain pharmacological and toxicological data for screening drugs and modeling disease.

STAR★METHODS

Detailed methods are provided in the online version of this paper and include the following:

- KEY RESOURCES TABLE
- RESOURCE AVAILABILITY
  - Lead contact
  - Materials availability
  - Data and code availability
- EXPERIMENTAL MODEL AND SUBJECT DETAILS
  - Animal models
  - Adult ventricular myocyte isolation (adult-CM)
  - Neonatal ventricular myocyte isolation (neonatal-CM)
  - Human-induced pluripotent stem cell-derived cardiomyocytes (hiPSC-CM)
- METHOD DETAILS
  - Overview of the software
  - Cell treatment
  - Microscopy system imaging
  - Image contractility analysis
  - Wave detection algorithms and data contractility analysis
- QUANTIFICATION AND STATISTICAL ANALYSIS

SUPPLEMENTAL INFORMATION

Supplemental information can be found online at https://doi.org/10.1016/j.crmeth.2021.100044.

ACKNOWLEDGMENTS

We thank professor Dr. Lívia Siman Gomes and Dr. Lucas Bleicher for guidance and support. This work was supported by CAPES, CNPq-Universal (423465/2018-0), FAPEMIG Rede de Pesquisa e Inovação Para Bioengenharia de Nanossistemas (RED-00282-16) and FAPEMIG Universal (APQ-01510-17). S.S. and M.Q.L.A. are recipients of CAPES PhD fellowships. C.A.T.F.M is a recipient of a CAPES-PRINT fellowship.

AUTHOR CONTRIBUTIONS

S.G., U.A., and S.S. conceived and led the project. M.Q.L.A., S.S., and N.J.d.F. developed the CONTRACTIONWAVE algorithm and GUI. D.B. and E.C. generated the hiPSC-CMs. I.C.G.J. isolated adult-CMs. S.S. isolated neonatal-CMs. S.S., A.P.A., V.P.T., and K.M. performed the drug screen and analyzed data. S.G., U.A., S.S., C.A.T.F.M., C.K., M.J.C.-S., A.K.S., O.N.M., and F.A.M.M. wrote and edited the manuscript. All authors critically reviewed and approved the final manuscript.

DECLARATION OF INTERESTS

The authors declare no competing interests.

Received: December 23, 2020
Revised: May 2, 2021
Accepted: June 14, 2021
Published: July 7, 2021

REFERENCES

Ballan, N., Shaheen, N., Keller, G.M., and Gepstein, L. (2020). Single-cell mechanical analysis of human pluripotent stem cell-derived cardiomyocytes for drug testing and pathophysiological studies. Stem Cell Reports *15*, 587–596. https://doi.org/10.1016/j.stemcr.2020.07.006.

Bedada, F.B., Wheelwright, M., and Metzger, J.M. (2016). Maturation status of sarcomere structure and function in human iPSC-derived cardiac myocytes. Biochim. Biophys. Acta - Mol. Cell Res. *1863*, 1829–1838. https://doi.org/10.1016/j.bbamcr.2015.11.005.

Belostotskaya, G., and Golovanova, T. (2014). Characterization of contracting cardiomyocyte colonies in the primary culture of neonatal rat myocardial cells: a model of in vitro cardiomyogenesis. Cell Cycle *13*, 910–918. https://doi.org/10.4161/cc.27768.

Berger, H.J., Prasad, S.K., Davidoff, A.J., Pimental, D., Ellingsen, O., Marsh, J.D., Smith, T.W., and Kelly, R.A. (1994). Continual electric field stimulation preserves contractile function of adult ventricular myocytes in primary culture. Am. J. Physiol. Circ. Physiol. *266*, H341–H349. https://doi.org/10.1152/ajpheart.1994.266.1.H341.

Birket, M.J., Ribeiro, M.C., Kosmidis, G., Ward, D., Leitoguinho, A.R., van de Pol, V., Dambrot, C., Devalla, H.D., Davis, R.P., Mastroberardino, P.G., et al. (2015). Contractile defect caused by mutation in MYBPC3 revealed under conditions optimized for human PSC-cardiomyocyte function. Cell Rep *13*, 733–745. https://doi.org/10.1016/j.celrep.2015.09.025.

Boudaoud, A., Burian, A., Borowska-Wykręt, D., Uyttewaal, M., Wrzalik, R., Kwiatkowska, D., Hamant, O., Borowska-Wykręt, D., Uyttewaal, M., Wrzalik, R., et al. (2014). FibrilTool, an ImageJ plug-in to quantify fibrillar structures in raw microscopy images. Nat. Protoc. *9*, 457–463. https://doi.org/10.1038/nprot.2014.024.

Boudreau-Béland, J., Duverger, J.E., Petitjean, E., Maguy, A., Ledoux, J., and Comtois, P. (2015). Spatiotemporal stability of neonatal rat cardiomyocyte monolayers spontaneous activity is dependent on the culture substrate. PLoS One *10*, e0127977. https://doi.org/10.1371/journal.pone.0127977.

Bourgonje, V.J.A.A., Vos, M.A., Ozdemir, S., Doisne, N., Acsai, K., Varro, A., Sztojkov-Ivanov, A., Zupko, I., Rauch, E., Kattner, L., et al. (2013). Combined Na^+/Ca^{2+} exchanger and L-type calcium channel block as a potential strategy to suppress arrhythmias and maintain ventricular function. Circ. Arrhythmia Electrophysiol. *6*, 371–379. https://doi.org/10.1161/CIRCEP.113.000322.

Bradski, G. (2000). The OpenCV Library (Dr. Dobb's Journal of Software Tools).

Burridge, P.W., Matsa, E., Shukla, P., Lin, Z.C., Churko, J.M., Ebert, A.D., Lan, F., Diecke, S., Huber, B., Mordwinkin, N.M., et al. (2014). Chemically defined generation of human cardiomyocytes. Nat. Methods *11*, 855–860. https://doi.org/10.1038/nmeth.2999.

Butler, L., Cros, C., Oldman, K.L., Harmer, A.R., Pointon, A., Pollard, C.E., and Abi-Gerges, N. (2015). Enhanced characterization of contractility in cardiomyocytes during early drug safety assessment. Toxicol. Sci. *145*, 396–406. https://doi.org/10.1093/toxsci/kfv062.

Chang, W.-T.T., Yu, D., Lai, Y.-C.C., Lin, K.-Y.Y., and Liau, I. (2013). Characterization of the mechanodynamic response of cardiomyocytes with atomic force microscopy. Anal. Chem. *85*, 1395–1400. https://doi.org/10.1021/ac3022532.

Chen-Izu, Y., Chen, L., Bányász, T., McCulle, S.L., Norton, B., Scharf, S.M., Agarwal, A., Patwardhan, A., Izu, L.T., and Balke, C.W. (2007). Hypertension-induced remodeling of cardiac excitation-contraction coupling in ventricular myocytes occurs prior to hypertrophy development. Am. J. Physiol. Circ. Physiol. *293*, H3301–H3310. https://doi.org/10.1152/ajpheart.00259.2007.

Chen, C.Y., Caporizzo, M.A., Bedi, K., Vite, A., Bogush, A.I., Robison, P., Heffler, J.G., Salomon, A.K., Kelly, N.A., Babu, A., et al. (2018). Suppression of detyrosinated microtubules improves cardiomyocyte function in human heart failure. Nat. Med. *24*, 1225–1233. https://doi.org/10.1038/s41591-018-0046-2.

Chou, B.-K., Mali, P., Huang, X., Ye, Z., Dowey, S.N., Resar, L.M., Zou, C., Zhang, Y.A., Tong, J., and Cheng, L. (2011). Efficient human iPS cell derivation by a non-integrating plasmid from blood cells with unique epigenetic

and gene expression signatures. Cell Res *21*, 518–529. https://doi.org/10.1038/cr.2011.12.

Clark, A. (2015). Pillow (PIL Fork) documentation. Readthedocs.https://buildmedia.readthedocs.org/media/pdf/pillow/latest/pillow.pdf.

Cruvinel, E., Ogusuku, I., Cerioni, R., Rodrigues, S., Gonçalves, J., Góes, M.E., Alvim, J.M., Silva, A.C., Lino, V.de S., Boccardo, E., et al. (2020). Long-term single-cell passaging of human iPSC fully supports pluripotency and high-efficient trilineage differentiation capacity. SAGE Open Med. *8*, 205031212096645. https://doi.org/10.1177/2050312120966456.

Czirok, A., Isai, D.G., Kosa, E., Rajasingh, S., Kinsey, W., Neufeld, Z., Rajasingh, J., Edina, K., Rajasingh, S., and Ki, W. (2017). Optical-flow based non-invasive analysis of cardiomyocyte contractility. Sci. Rep. *7*, 10404. https://doi.org/10.1038/s41598-017-10094-7.

Delbridge, L.M.D., and Roos, K.P. (1997). Optical methods to evaluate the contractile function of unloaded isolated cardiac myocytes. J. Mol. Cell. Cardiol. *29*, 11–25. https://doi.org/10.1006/jmcc.1996.0247.

Farneback, G. (2003). Two-frame motion estimation based on polynomial expansion. Lecture Notes Computer Sci., 363–370. https://doi.org/10.1007/3-540-45103-X_50.

Goméz, A.M. (1997). Defective excitation-contraction coupling in experimental cardiac hypertrophy and heart failure. Science *276*, 800–806. https://doi.org/10.1126/science.276.5313.800.

Gong, J.Q.X., and Sobie, E.A. (2018). Population-based mechanistic modeling allows for quantitative predictions of drug responses across cell types. Npj Syst. Biol. Appl. *4*, 11. https://doi.org/10.1038/s41540-018-0047-2.

Gorelik, J., Ali, N.N., Shevchuk, A.I., Lab, M., Williamson, C., Harding, S.E., and Korchev, Y.E. (2006). Functional characterization of embryonic stem cell-derived cardiomyocytes using scanning ion conductance microscopy. Tissue Eng. *12*, 657–664. https://doi.org/10.1089/ten.2006.12.657.

Grune, T., Ott, C., Häseli, S., Höhn, A., and Jung, T. (2019). The "MYOCYTER" – convert cellular and cardiac contractions into numbers with ImageJ. Sci. Rep. *9*, 1–13. https://doi.org/10.1038/s41598-019-51676-x.

Guatimosim, S., Amaya, M.J., Guerra, M.T., Aguiar, C.J., Goes, A.M., Gómez-Viquez, N.L., Rodrigues, M.A., Gomes, D.A., Martins-Cruz, J., Lederer, W.J., et al. (2008). Nuclear Ca^{2+} regulates cardiomyocyte function. Cell Calcium *44*, 230–242. https://doi.org/10.1016/j.ceca.2007.11.016.

Guatimosim, S., Dilly, K., Santana, L.F., Saleet Jafri, M., Sobie, E.a, and Lederer, W.J. (2002). Local Ca(2+) signaling and EC coupling in heart: Ca(2+) sparks and the regulation of the [Ca(2+)](i) transient. J. Mol. Cell. Cardiol. *34*, 941–950. https://doi.org/10.1006/jmcc.2002.2032.

Harary, I., and Farley, B. (1960). In vitro studies of single isolated beating heart cells. Science *131*, 1674–1675. https://doi.org/10.1126/science.131.3414.1674.

Harmer, A.R.R., Abi-Gerges, N., Morton, M.J.J., Pullen, G.F.F., Valentin, J.P.P., and Pollard, C.E.E. (2012). Validation of an in vitro contractility assay using canine ventricular myocytes. Toxicol. Appl. Pharmacol. *260*, 162–172. https://doi.org/10.1016/j.taap.2012.02.007.

Harris, C.R., Millman, K.J., van der Walt, S.J., Gommers, R., Virtanen, P., Cournapeau, D., Wieser, E., Taylor, J., Berg, S., Smith, N.J., et al. (2020). Array programming with NumPy. Nature *585*, 357–362. https://doi.org/10.1038/s41586-020-2649-2.

Haworth, R.A., Griffin, P., Saleh, B., Goknur, A.B., and Berkoff, H.A. (1987). Contractile function of isolated young and adult rat heart cells. Am. J. Physiol. Circ. Physiol. *253*, H1484–H1491. https://doi.org/10.1152/ajpheart.1987.253.6.H1484.

Hayakawa, T., Kunihiro, T., Ando, T., Kobayashi, S., Matsui, E., Yada, H., Kanda, Y., Kurokawa, J., and Furukawa, T. (2014). Image-based evaluation of contraction–relaxation kinetics of human-induced pluripotent stem cell-derived cardiomyocytes: correlation and complementarity with extracellular electrophysiology. J. Mol. Cell. Cardiol. *77*, 178–191. https://doi.org/10.1016/j.yjmcc.2014.09.010.

Hissa, B., Oakes, P.W., Pontes, B., Ramírez-San Juan, G., and Gardel, M.L. (2017). Cholesterol depletion impairs contractile machinery in neonatal rat cardiomyocytes. Sci. Rep. *7*, 43764. https://doi.org/10.1038/srep43764.

Hossain, M.M., Shimizu, E., Saito, M., Ramachandra Rao, S., Yamaguchi, Y., and Tamiya, E. (2010). Non-invasive characterization of mouse embryonic stem cell derived cardiomyocytes based on the intensity variation in digital beating video. Analyst *135*, 1624. https://doi.org/10.1039/c0an00208a.

Huebsch, N., Loskill, P., Mandegar, M.A., Marks, N.C., Sheehan, A.S., Ma, Z., Mathur, A., Nguyen, T.N., Yoo, J.C., Judge, L.M., et al. (2015). Automated video-based analysis of contractility and calcium flux in human-induced pluripotent stem cell-derived cardiomyocytes cultured over different spatial scales. Tissue Eng. Part C Methods *21*, 467–479. https://doi.org/10.1089/ten.tec.2014.0283.

Hunter, J.D. (2007). Matplotlib: a 2D graphics environment. Comput. Sci. Eng. *9*, 90–95. https://doi.org/10.1109/MCSE.2007.55.

Jesus, I.C.G., Mesquita, T.R.R., Monteiro, A.L.L., Parreira, A.B., Santos, A.K., Coelho, E.L.X., Silva, M.M., Souza, L.A.C., Campagnole-Santos, M.J., Santos, R.S., et al. (2020). Alamandine enhances cardiomyocyte contractility in hypertensive rats through a nitric oxide-dependent activation of CaMKII. Am. J. Physiol. - Cell Physiol. *318*, C740–C750. https://doi.org/10.1152/ajpcell.00153.2019.

Jung, G., Fajardo, G., Ribeiro, A.J.S., Kooiker, K.B., Coronado, M., Zhao, M., Hu, D., Reddy, S., Kodo, K., Sriram, K., et al. (2016). Time-dependent evolution of functional vs. remodeling signaling in induced pluripotent stem cell-derived cardiomyocytes and induced maturation with biomechanical stimulation. FASEB J. *30*, 1464–1479. https://doi.org/10.1096/fj.15-280982.

Khan, M., Xu, Y., Hua, S., Johnson, J., Belevych, A., Janssen, P.M.L., Gyorke, S., Guan, J., and Angelos, M.G. (2015). Evaluation of changes in morphology and function of human induced pluripotent stem cell derived cardiomyocytes (HiPSC-CMs) cultured on an aligned-nanofiber cardiac patch. PLoS One *10*, e0126338. https://doi.org/10.1371/journal.pone.0126338.

Kodo, K., Ong, S.-G.G., Jahanbani, F., Termglinchan, V., Hirono, K., InanlooRahatloo, K., Ebert, A.D., Shukla, P., Abilez, O.J., Churko, J.M., et al. (2016). iPSC-derived cardiomyocytes reveal abnormal TGF-β signalling in left ventricular non-compaction cardiomyopathy. Nat. Cell Biol. *18*, 1031–1042. https://doi.org/10.1038/ncb3411.

Korhonen, T., Hänninen, S.L., and Tavi, P. (2009). Model of excitation-contraction coupling of rat neonatal ventricular myocytes. Biophys. J. *96*, 1189–1209. https://doi.org/10.1016/j.bpj.2008.10.026.

Kovács, Á., Fülöp, G.Á., Kovács, A., Csípő, T., Bódi, B., Priksz, D., Juhász, B., Beke, L., Hendrik, Z., Méhes, G., et al. (2016). Renin overexpression leads to increased titin-based stiffness contributing to diastolic dysfunction in hypertensive mRen2 rats. Am. J. Physiol. Circ. Physiol. *310*, H1671–H1682. https://doi.org/10.1152/ajpheart.00842.2015.

Lahti, A.L., Kujala, V.J., Chapman, H., Koivisto, A.-P., Pekkanen-Mattila, M., Kerkela, E., Hyttinen, J., Kontula, K., Swan, H., Conklin, B.R., et al. (2012). Model for long QT syndrome type 2 using human iPS cells demonstrates arrhythmogenic characteristics in cell culture. Dis. Model. Mech. *5*, 220–230. https://doi.org/10.1242/dmm.008409.

Lan, F., Lee, A.S., Liang, P., Sanchez-Freire, V., Nguyen, P.K., Wang, L., Han, L., Yen, M., Wang, Y., Sun, N., et al. (2013). Abnormal calcium handling properties underlie familial hypertrophic cardiomyopathy pathology in patient-specific induced pluripotent stem cells. Cell Stem Cell *12*, 101–113. https://doi.org/10.1016/j.stem.2012.10.010.

Langheinrich, M. (1996). The hypertensive Ren-2 transgenic rat TGR (mREN2) 27 in hypertension research characteristics and functional aspects. Am. J. Hypertens. *9*, 506–512. https://doi.org/10.1016/0895-7061(95)00400-9.

Leung, A.F. (1982). Laser diffraction of single intact cardiac muscle cells at rest. J. Muscle Res. Cell Motil. *3*, 399–418. https://doi.org/10.1007/BF00712091.

Li, Q., Ni, R., Hong, H., Goh, K.Y., Rossi, M., Fast, V.G., and Zhou, L. (2017). Electrophysiological properties and viability of neonatal rat ventricular myocyte cultures with inducible ChR2 expression. Sci. Rep. *7*, 1531. https://doi.org/10.1038/s41598-017-01723-2.

Lian, X., Zhang, J., Azarin, S.M., Zhu, K., Hazeltine, L.B., Bao, X., Hsiao, C., Kamp, T.J., and Palecek, S.P. (2013). Directed cardiomyocyte differentiation from human pluripotent stem cells by modulating Wnt/β-catenin signaling under fully defined conditions. Nat. Protoc. *8*, 162–175. https://doi.org/10.1038/nprot.2012.150.

Lieben Louis, X., Raj, P., Meikle, Z., Yu, L., Susser, S.E., MacInnis, S., Duhamel, T.A., Wigle, J.T., and Netticadan, T. (2019). Resveratrol prevents palmitic-acid-induced cardiomyocyte contractile impairment. Can. J. Physiol. Pharmacol. *97*, 1132–1140. https://doi.org/10.1139/cjpp-2019-0051.

Louch, W.E., Koivumäki, J.T., and Tavi, P. (2015). Calcium signalling in developing cardiomyocytes: implications for model systems and disease. J. Physiol. *593*, 1047–1063. https://doi.org/10.1113/jphysiol.2014.274712.

Lundh, F. (1999). An introduction to tkinter.www.Pythonware.com/Library/Tkinter/Introduction/Index.htm.

Maddah, M., Heidmann, J.D., Mandegar, M.A., Walker, C.D., Bolouki, S., Conklin, B.R., and Loewke, K.E. (2015). A non-invasive platform for functional characterization of stem-cell-derived cardiomyocytes with applications in cardiotoxicity testing. Stem Cell Reports *4*, 621–631. https://doi.org/10.1016/j.stemcr.2015.02.007.

McKinney, W., (2010). Data structures for statistical computing in Python. pp. 56–61. https://doi.org/10.25080/Majora-92bf1922-00a

Mozaffarian, D., Benjamin, E.J., Go, A.S., Arnett, D.K., Blaha, M.J., Cushman, M., Das, S.R., Ferranti, S. De, Després, J.P., Fullerton, H.J., et al. (2016). Heart disease and stroke statistics—2016 update a report from the American Heart Association. Circulation. https://doi.org/10.1161/CIR.0000000000000350.

Mullins, J.J., Peters, J., and Ganten, D. (1990). Fulminant hypertension in transgenic rats harbouring the mouse Ren-2 gene. Nature *344*, 541–544. https://doi.org/10.1038/344541a0.

Nguyen, N., Nguyen, W., Nguyenton, B., Ratchada, P., Page, G., Miller, P.E., Ghetti, A., and Abi-Gerges, N. (2017). Adult human primary cardiomyocyte-based model for the simultaneous prediction of drug-induced inotropic and pro-arrhythmia risk. Front. Physiol. *8*. https://doi.org/10.3389/fphys.2017.01073.

Pasqualin, C., Gannier, F., Yu, A., Malécot, C.O., Bredeloux, P., and Maupoil, V. (2016). SarcOptiM for ImageJ: high-frequency online sarcomere length computing on stimulated cardiomyocytes. Am. J. Physiol. Physiol. *311*, C277–C283. https://doi.org/10.1152/ajpcell.00094.2016.

Penitente, A.R., Novaes, R.D., Silva, M.F.M.E., Silva, M.F.M.E., Quintão-Júnior, J.F., Guatimosim, S., Cruz, J.S., Chianca-, D.A., Jr., Natali, A.J., and Neves, C.A. (2014). Basal and β-adrenergic cardiomyocytes contractility dysfunction induced by dietary protein restriction is associated with downregulation of SERCA2a expression and disturbance of endoplasmic reticulum Ca^{2+} regulation in rats. Cell. Physiol. Biochem. *34*, 443–454. https://doi.org/10.1159/000363013.

Pointon, A., Pilling, J., Dorval, T., Wang, Y., Archer, C., and Pollard, C. (2017). From the cover: high-throughput imaging of cardiac microtissues for the assessment of cardiac contraction during drug discovery. Toxicol. Sci. *155*, 444–457. https://doi.org/10.1093/toxsci/kfw227.

Ramadan, M., Sherman, M., Jaimes, R., Chaluvadi, A., Swift, L., and Posnack, N.G. (2018). Disruption of neonatal cardiomyocyte physiology following exposure to bisphenol-a. Sci. Rep. *8*, 7356. https://doi.org/10.1038/s41598-018-25719-8.

Ren, J., and Wold, L.E. (2001). Measurement of cardiac mechanical function in isolated ventricular myocytes from rats and mice by computerized video-based imaging. Biol. Proced. Online *3*, 43–53. https://doi.org/10.1251/bpo22.

Ribeiro, A.J.S., Ang, Y.-S., Fu, J.-D., Rivas, R.N., Mohamed, T.M.A., Higgs, G.C., Srivastava, D., and Pruitt, B.L. (2015). Contractility of single cardiomyocytes differentiated from pluripotent stem cells depends on physiological shape and substrate stiffness. Proc. Natl. Acad. Sci. *112*, 12705–12710. https://doi.org/10.1073/pnas.1508073112.

Rohr, S., Schölly, D.M., and Kléber, A.G. (1991). Patterned growth of neonatal rat heart cells in culture. Morphological and electrophysiological characterization. Circ. Res. *68*, 114–130. https://doi.org/10.1161/01.RES.68.1.114.

Sala, L., Van Meer, B.J., Tertoolen, L.G.J., Bakkers, J., Bellin, M., Davis, R.P., Denning, C., Dieben, M.A.E., Eschenhagen, T., Giacomelli, E., et al. (2018). Musclemotion: a versatile open software tool to quantify cardiomyocyte and cardiac muscle contraction in vitro and in vivo. Circ. Res. *122*, e5–e16. https://doi.org/10.1161/CIRCRESAHA.117.312067.

Schick, R., Mekies, L.N., Shemer, Y., Eisen, B., Hallas, T., Ben Jehuda, R., Ben-Ari, M., Szantai, A., Willi, L., Shulman, R., et al. (2018). Functional abnormalities in induced pluripotent stem cell-derived cardiomyocytes generated from titin-mutated patients with dilated cardiomyopathy. PLoS One *13*, e0205719. https://doi.org/10.1371/journal.pone.0205719.

Schindelin, J., Rueden, C.T., Hiner, M.C., and Eliceiri, K.W. (2015). The ImageJ ecosystem: an open platform for biomedical image analysis. Mol. Reprod. Dev. *82*, 518–529. https://doi.org/10.1002/mrd.22489.

Schneider, C.A., Rasband, W.S., and Eliceiri, K.W. (2012). NIH Image to ImageJ: 25 years of image analysis. Nat. Methods *9*, 671–675. https://doi.org/10.1038/nmeth.2089.

Shevchuk, A.I., Gorelik, J., Harding, S.E., Klenerman, D., Korchev, Y.E., Lab, M.J., Klenerman, D., and Korchev, Y.E. (2001). Simultaneous measurement of Ca^{2+} and cellular dynamics: combined scanning ion conductance and optical microscopy to study contracting cardiac myocytes. Biophys. J. *81*, 1759–1764. https://doi.org/10.1016/S0006-3495(01)75826-2.

Slotkin, T.A., Lappi, S.E., and Seidler, F.J. (1995). β-Adrenergic control of c-fos expression in fetal and neonatal rat tissues: relationship to cell differentiation and teratogenesis. Toxicol. Appl. Pharmacol. *133*, 188–195. https://doi.org/10.1006/taap.1995.1141.

Song, L.-S., Pi, Y., Kim, S.-J., Yatani, A., Guatimosim, S., Kudej, R.K., Zhang, Q., Cheng, H., Hittinger, L., Ghaleb, B., et al. (2005). Paradoxical cellular Ca^{2+} signaling in severe but compensated canine left ventricular hypertrophy. Circ. Res. *97*, 457–464. https://doi.org/10.1161/01.RES.0000179722.79295.d4.

Steadman, B.W.W., Moore, K.B.B., Spitzer, K.W.W., and Bridge, J.H.B.H.B. (1988). A video system for measuring motion in contracting heart cells. IEEE Trans. Biomed. Eng. *35*, 264–272. https://doi.org/10.1109/10.1375.

Stern, H.C., Matthews, J.H., and Belz, G.G. (1986). Intrinsic and reflex actions of verapamil and nifedipine: assessment in normal subjects by noninvasive techniques and autonomic blockade. Eur. J. Clin. Pharmacol. *29*, 541–547. https://doi.org/10.1007/BF00635890.

Tofoli, F.A., Dasso, M., Morato-Marques, M., Nunes, K., Pereira, L.A., da Silva, G.S., Fonseca, S.A.S., Costas, R.M., Santos, H.C., da Costa Pereira, A., et al. (2016). Increasing the genetic admixture of available lines of human pluripotent stem cells. Sci. Rep. *6*, 34699. https://doi.org/10.1038/srep34699.

van Rossum, G. (1995). Python tutorial, May 1995. CWI Rep., 1–65, CS-R9526.

Virtanen, P., Gommers, R., Oliphant, T.E., Haberland, M., Reddy, T., Cournapeau, D., Burovski, E., Peterson, P., Weckesser, W., Bright, J., et al. (2020). SciPy 1.0: fundamental algorithms for scientific computing in Python. Nat. Methods *17*, 261–272. https://doi.org/10.1038/s41592-019-0686-2.

Wang, G., McCain, M.L., Yang, L., He, A., Pasqualini, F.S., Agarwal, A., Yuan, H., Jiang, D., Zhang, D., Zangi, L., et al. (2014). Modeling the mitochondrial cardiomyopathy of Barth syndrome with induced pluripotent stem cell and heart-on-chip technologies. Nat. Med. *20*, 616–623. https://doi.org/10.1038/nm.3545.

Wang, H., Sheehan, R.P., Palmer, A.C., Everley, R.A., Boswell, S.A., Ron-Harel, N., Ringel, A.E., Holton, K.M., Jacobson, C.A., Erickson, A.R., et al. (2019). Adaptation of human iPSC-derived cardiomyocytes to tyrosine kinase inhibitors reduces acute cardiotoxicity via metabolic reprogramming. Cell Syst *8*, 412–426.e7. https://doi.org/10.1016/j.cels.2019.03.009.

STAR★METHODS

KEY RESOURCES TABLE

REAGENT or RESOURCE	SOURCE	IDENTIFIER
Antibodies		
Anti-TNNT2	Thermo Fisher Scientific	Cat#MA5-12960; RRID: AB_11000742
Anti-TNNI3	DSHB	Cat#TI-4; RRID: AB_10573815
Bacterial and virus strains		
pEB-C5	Chou et al., 2011	Cat#Addgene 28213; RRID: Addgene_28213
pEB-Tg	Chou et al., 2011	Cat#Addgene 28220; RRID: Addgene_28220
Chemicals, peptides, and recombinant proteins		
Isoproterenol	Sigma-Aldrich	Cat#I6504
Verapamil Hydrochloride	Sigma-Aldrich	Cat#V4629
Trypsin-EDTA solution	Sigma-Aldrich	Cat#T4299
Cytosine β-D-arabinofuranoside	Sigma-Aldrich	Cat#C1768
Bovine Serum, heat inactivated, New Zealand origin - Gibco®	Thermo Fisher Scientific	Cat#26170035
Trypsin inhibitor from Glycine max (soybean)	Sigma-Aldrich	Cat#T6522
Penicillin-Streptomycin	Sigma-Aldrich	Cat#P4333
Insulin from bovine pancreas	Sigma-Aldrich	Cat#I5500
Bovine Serum Albumin	Sigma-Aldrich	Cat#A7906
Collagenase, Type 2	Worthington Biochemical Corporation	Cat#L5004176
Y27632	Cayman Chemical	Cat#10005583
B27 supplement without insulin	Thermo Fisher Scientific	Cat#1895601
CHIR99021	Merck Millipore Sigma	Cat#361571
B27 supplement	Thermo Fisher Scientific	Cat#17504044
BMP4	R&D Systems	Cat#314-BP-010
KY2111	Cayman Chemical	Cat#14315
XAV939	Cayman Chemical	Cat#13596
DPBS 35% BSA	Merck Millipore Sigma	Cat#A7979
Plasmocin	InvivoGen	Cat#ANT-MPT
Critical commercial assays		
Human CD34+ Cell Nucleofector kit	Lonza	VPA-1003
Deposited data		
Raw and analyzed data	This paper	N/A
Sample data is available from Mendeley Data at the following doi	This paper	https://doi.org/10.17632/hswwzgw6rp.1
Experimental models: Cell lines		
human-induced pluripotent stem cell-derived cardiomyocytes (hiPSC-CM)	Pluricell Biotech®	https://www.pluricellbiotech.com.br/
Experimental models: Organisms/strains		
Mouse: C57BL/6	Animal Facility UFMG	https://www.jax.org/strain/000664
Wistar Rat	Animal Facility of the Department of Physiology and Biophysics ICB-UFMG	N/A
Sprague-Dawley rats	Laboratory of Hypertension ICB-UFMG	N/A
Hypertensive transgenic rat: TGR(mREN2)27	Laboratory of Hypertension ICB-UFMG	N/A

(*Continued on next page*)

Continued

REAGENT or RESOURCE	SOURCE	IDENTIFIER
Software and algorithms		
CONTRACTIONWAVE Code repository	This paper	https://github.com/marceloqla/ContractionWavePy
CONTRACTIONWAVE executable file	This paper	https://sites.icb.ufmg.br/cardiovascularrc/contractionwave https://doi.org/10.17632/hswwzgw6rp.1
Python 3.6.9	van Rossum, 1995	https://www.python.org/
Numpy	Harris et al., 2020	https://github.com/numpy/numpy
Pandas	McKinney, 2010	https://github.com/pandas-dev/pandas
Matplotlib	Hunter, 2007	https://github.com/matplotlib/matplotlib
Opencv	Bradski, 2000	https://github.com/opencv/opencv
Ttkthemes	https://pypi.org/project/ttkthemes/	https://github.com/TkinterEP/ttkthemes
Tkinter	Lundh, 1999	https://www.python.org/
Pillow	Clark, 2015	https://github.com/python-pillow/Pillow
Xlsxwriter	https://pypi.org/project/XlsxWriter/	https://github.com/jmcnamara
Psutil	https://pypi.org/project/psutil/	https://github.com/giampaolo/psutil
SciPy	Virtanen et al., 2020	https://github.com/scipy/scipy
PyInstaller	https://www.pyinstaller.org/	https://github.com/pyinstaller/pyinstaller
Ionicons		https://ionicons.com/
ImageJ	Schneider et al., 2012	https://imagej.nih.gov/ij/
Other		
CMOS camera	EPIX, Inc	SILICON VIDEO ® 642M
Nikon Eclipse Ti-E inverted microscope	Nikon	Ti-E
ChamlideIC-CU Incubator	Live Cell Instrument, Nowan-gu, Korea	109

RESOURCE AVAILABILITY

Lead contact

Further information and requests for resources and reagents should be directed to and will be fulfilled by the Lead Contact, Silvia Guatimosim, guatimosim@icb.ufmg.br

Materials availability

This study did not generate new materials.

Data and code availability

CONTRACTIONWAVE is free and open-source, distributed under the terms of the GNU General Public License version 2, and its source code is available at: https://github.com/marceloqla/ContractionWavePy.

Sample data of this study are available at the Mendeley Data:
https://doi.org/10.17632/hswwzgw6rp.1

Given large file sizes, the image data that supports the findings in supplemental figures of this study are available from the lead contact upon request.

CONTRACTIONWAVE can be installed from an executable file for **Windows or Ubuntu** (see section 3.1 of the User Manual provided as Methods S1) or from Anaconda environment installation for **Windows, Ubuntu or Mac-OS** (see section 3.2 of the User Manual provided as Methods S1).

Additional information about the CONTRACTIONWAVE installation and how to process data can be found in the User Manual (Methods S1).

EXPERIMENTAL MODEL AND SUBJECT DETAILS

Animal models

For this study, we used male C57BL/6 Mice 10-12 weeks of age (n=3), neonatal (P1-3) Wistar rats (n=10), male Sprague-Dawley rats 10-14 week old (SD, n=3), and heterozygous TGR (mREN2)27 (n=3) rats. The rats used in this study were obtained from the breeding

colony established at the animal facility of the Laboratory of Hypertension, Institute of Biological Sciences/UFMG, and the mice were obtained from the UFMG animal facility. Experiments were performed according to protocols approved by the Institutional Animal Care and Use Committee at Universidade Federal de Minas Gerais (UFMG). The study followed the National Institutes of Health (NIH) Guide for the Care and Use of Laboratory Animals (CEUA 138/2018).

Adult ventricular myocyte isolation (adult-CM)

Cardiomyocytes from adult mice were isolated according to the methodology as previously described (Guatimosim et al., 2002). Briefly, the heart was rapidly removed and perfused retrogradely by the Langendorff method with Ca^{2+} free modified Tyrode's solution. Subsequently, the heart was perfused with Ca^{2+} free modified Tyrode's solution containing 50 μmol/L CaCl2 and collagenase type 2 (1 mg/ml) for approximately 12 minutes. The ventricular chambers were separated and submitted to mechanical digestion. It is then filtered to remove tissue that has not been digested. The extracellular concentration of Ca^{2+} was increased after three cycles of centrifugation and exchange of buffer, reaching 500 μmol/L at the end of the process. Soon after, the cells were again centrifuged and maintained in Tyrode's solution.

Neonatal ventricular myocyte isolation (neonatal-CM)

Cardiac tissue was removed from 1- to 3-day-old Wistar rats, as previously described by Guatimosim et al., 2008. In brief, the collagenase type 2 enzyme was used to digest the heart tissue. Isolated neonatal rat cardiomyocytes were resuspended in Dulbecco's modified Eagle's medium (DMEM) supplemented with 10% fetal bovine serum (FBS), 100 U/ml penicillin, and 100 μg/ml streptomycin, and replated in 75-cm^2 flasks for 2h. The cells were then plated into fibronectin-coated culture dishes and incubated at 37°C in a 5% CO2 incubator. One day after plating, cells were rinsed with DMEM plus serum and fed for another 48 h with regular culture medium, now including 20 μg/ml cytosine-D-arabinofuranoside to inhibit the growth of noncardiomyocytes. The cultured cells were used in experiments on the fourth day of culture.

Human-induced pluripotent stem cell-derived cardiomyocytes (hiPSC-CM)

Human-Induced pluripotent stem cell (hiPSCs) reprogramming was performed as described in Tofoli et al., 2016. Briefly, hiPSCs lines were derived from erythroblasts by transfection with plasmids pEB-C5 and pEB-Tg using the Human CD34+ nucleofector kit and the Nucleofector II device, following manufacturer's instructions. One clone (ACP5) was selected, expanded, and presented several pluripotent Stem Cells markers OCT4, NANOG, SOX2, and SSEA4, and did not presently karyotype aberrations after long term cell cultivation (Cruvinel et al., 2020). hiPSCs were differentiated using a monolayer directed differentiation method modified from previous reports (Burridge et al., 2014; Lian et al., 2013). hiPSCs were grown in feeder-free conditions until they reached 60%–70% confluence. Cells were singularized, counted, and plated (2.5 x 105 cells/cm^2) with E8 medium (Thermo Fisher, USA) with 10 μM of Y27632 (Cayman Chemical, USA). E8 medium was changed daily until cells reached 100% confluence. This day was considered as differentiation day 0 and the medium was changed to RPMI 1640 supplemented with 1x B27 supplement (Thermo Fisher, USA) without insulin (RB-) and 4 μM CHIR99021 (Merck Millipore Sigma, USA). 24 hours later, the medium was changed to RB- supplemented with 10 ng/mL BMP4 (R&D Systems, USA). On day 2, the medium was changed to fresh RB- supplemented with 2.5 μM KY2111 and XAV939 (both from Cayman Chemical, USA). On day 4 and every two days, the medium was changed to fresh RPMI supplemented with 213 μg/ml Ascorbic Acid 2- phosphate (Sigma Aldrich, USA), 500 μg/ml DPBS 35% BSA, and 2 μg/ml Plasmocin (InvivoGen, USA). Cells were cultivated for 15 days, passed with Trypsin EDTA (Thermo Fisher, USA). After Trypsin inactivation, cells were centrifuged and resuspended in RPMI supplemented with B27 supplement and 10 μM of Y27632 and plated at specific experiment confluence. This protocol generates a population of cardiomyocytes with purity above 90%. The cardiomyocytes used in the experiments from this manuscript showed purity above 98% by troponin-specific cardiac marker TNNT2 and more than 94% for mature Troponin I (TNNI3) (Figure S5). All cells (hiPSCs and cardiomyocytes) were checked for the absence of mycoplasma.

METHOD DETAILS

Overview of the software

CONTRACTIONWAVE (CW) is a software developed in Python Programming Language that allows the user to visualize, quantify, and analyze cell contractility parameters in a simple and intuitive format. The software enables the user to acquire membrane kinetics data of cell contractility during contraction-relaxation cycles through image capture and a dense optical flow algorithm. Both methods and software were developed using multidisciplinary knowledge, which resulted in a robust data extraction protocol. For details on step-by-step software instructions, see Methods S1: CONTRACTIONWAVE User manual v1.0, Related to STAR Methods.

Cell treatment

The drugs used in this study were purchased by Sigma-Aldrich: Isoproterenol and Verapamil Hydrochloride. The cells were incubated with isoproterenol or verapamil to perform a concentration-response curve. The incubation time was 5 min, with a variation between 5 and 15 min for image acquisition.

Microscopy system imaging

A high-speed digital CMOS camera (SILICON VIDEO ® 642M, EPIX, Inc) was coupled to a Nikon Eclipse Ti-E inverted microscope, brightfield microscopy, containing a 40x objective (Nikon Japan, 0.55 numerical aperture and 2.1mm working distance). In the microscope stage, an incubator (model ChamlideIC-CU: 109, Live Cell Instrument, Nowan-gu, Korea) was added that maintains uniform temperature (37°C) and humidity (60%) levels for adult-CM and also adding CO2 (5%) to neonatal-CM and hiPSC-CM. Adult cardiomyocytes were stimulated electrically by platinum electrodes (1Hz, 30V) with pulses of 5 ms duration. The image sequence was recorded at 200fps over 1min for adult-CM and 100fps over 15s for neonatal-CM and hiPSC-CM, with a resolution of 640x200 pixels and 640x480 respectively. The image pixel size was 0.25 μm/pixel with a depth of 8 bits.

Image contractility analysis

To detect cell contraction movement, we used the Dense Optical Flow methodology, which is based on the principles of optical flow, using the Gunnar Farneback algorithm (Farneback, 2003) to detect the movement of all points between a pair of images. CONTRACTIONWAVE supports various image types (Methods S1), and to obtain the best quality results, we used Tiff-8bit type images. We apply the Optical flow algorithm to a movie of a contractile cell with several frames F, and the image size n x m to obtain the magnitude of the displacement of a pixel between two frames. From the displacement for each pixel, we average to obtain a magnitude of the displacement for each frame (*i*) (i = [1, 2,..., F]) (Equation 1).

$$Avg.Mag(i) = \frac{1}{nxm} x \sum_{1}^{n} \sum_{1}^{m} |OpticalFlow(n, m, i)| \quad \text{(Equation 1)}$$

The displacement for each frame was obtained from the average of the magnitude of the displacement of each pixel in the image, converted to the actual speed multiplying the frame rate and pixel size (Equation 2), and then plotted as a function of time.

$$Speed(i) = Avg.MagxpixelFPS \quad \text{(Equation 2)}$$

Wave detection algorithms and data contractility analysis

A peak-detection algorithm was developed to measure contractility parameters over time. Maximum contraction Speed (MCS) and Maximum Relaxation Speed (MRS) are the two positive peaks spanning a central valley. The Minimum Speed Point is the minimum value of this valley between the MCS and MRS. To determine the return to baseline, a portion of the waveform after MRS (PArea, set to 0.9 as default) below a threshold (W) is fitted by a single exponential decay function. Return to baseline is the point in which a fraction of the total area fitted to an exponential curve, has reached a limit (PStop), set to 0.35 as default which can be changed by the user. Briefly, to detect the main parameters of the contractility we define four constants, W (speed median), Δ (mean of the speed points above W), PStop, and PArea (multiplication factors to adjusted parameters obtained by the exponential decay curve, to define the end of the contractility). All these parameters are defined from automated values estimated on optimal test cases or can be defined from user input to improve the fit to the data and their condition.

$$W = median[Speed(i)] if\ wave\ Max\ filter\ input \quad \text{(Equation 3)}$$

$$\Delta = mean[Speed(i)] > W \ \ if\ delta\ input \quad \text{(Equation 4)}$$

$$PStop = 0.9(default) \ \ if\ fraction\ of\ exp.AUC\ input \ \ |0 < input < 1| \quad \text{(Equation 5)}$$

$$PArea = 0.35(default) \ \ if\ fraction\ of\ wave\ Max\ area\ inpu \ \ |0 < input < 1| \quad \text{(Equation 6)}$$

The wave definition algorithm can be defined by the following steps:

First, we detect the pairs of peaks corresponding to possible MCS and MRS. These peaks are defined as the maximum points above W around a valley defined by Δ (Equation 4). To do that we adapted the peakdet algorithms from [http://billauer.co.il/peakdet.html]

A search algorithm is then applied for each pair of maximum points (MCS, MRS). A contraction initiation point is assigned from the closest local minimum point preceding MCS. The lowest average *speed* value between MCS and MRS is defined as the Minimum Speed point.

The Return to the baseline point is obtained by an exponential fit of the decaying curve after the maximum relaxation speed (MRS) (Equation 7). Since all values below W following the MRS can be used in this fit we included a parameter PArea (Equation 6) that allows subsetting the data to be fitted to possibly exclude any values belonging to the start of the next wave which could bias the regression.

$$exp.fit(afterMRS) = Lev.Marquardt\left(Ae^{-Bx} + c\right) \quad \text{(Equation 7)}$$

The total area under the decaying curve for the fitted exponential is then calculated:

$$A = \int exp.fit(afterMRS) \quad \text{(Equation 8)}$$

The Return to the baseline point is determined to be the first point above the proportion of the calculated area PStop (Equation 5). The search algorithm then skips to the next pair of maximums, detecting all possible waves for the current values of the four constants. An example of the detected points is shown in Figures 2A, S2B, and S2C.

Various parameters regarding Time, Speed, and the Area under the curve are calculated and averaged for all the user-selected waves (as seen in Figure S2C).

QUANTIFICATION AND STATISTICAL ANALYSIS

Data are presented as mean ± SEM of at least 3 independent experiments. For statistical comparison, we used Student's t-test, One-Way ANOVA followed by Dunnett's Multiple Comparison post hoc test. The level of significance was set to values of $p<0.05$.